Bio-Based and Chemically Recyclable Vitrimers from Poly(lactide) and Isosorbide Diglycidyl Ether

ACS Sustainable Chemistry & Engineering

pubs.acs.org/journal/ascecg

Research Article

Bio-Based and Chemically Recyclable Vitrimers from Poly(lactide) and Isosorbide Diglycidyl Ether

Licia Gaeta, Michele Gammino, Camilla Noè, Maria Gentile, Roberto Scaffaro,* and Claudio Pellecchia*

Cite This: *ACS Sustain. Chem. Eng.* 2026, 14, 12997−13012

Read Online

ACCESS | Metrics & More | Article Recommendations | Supporting Information

ABSTRACT: Bio-based and chemically recyclable vitrimer networks were synthesized from star-shaped poly(lactic acid) (PLA) oligomers and isosorbide diglycidyl ether (DGEIs). Hydroxyl-terminated 4- and 6-arm PLA oligomers were functionalized with carboxylic acid end-groups to improve reactivity with DGEIs. Crosslinking in the presence of $Zn(OAc)_2$ at 180 °C yielded homogeneous thermoset films with high gel fractions (>90%). Rheological and DSC analyses demonstrated temperature- dependent curing kinetics and rapid network formation. Mechanical testing revealed high stiffness in the GPa range with relatively low elongation at break, consistent with a highly crosslinked PLA-based thermoset architecture. Dynamic mechanical analysis and stress relaxation experiments confirmed vitrimeric behavior governed by thermally activated transesterification reactions, with Arrhenius-type dependence of relaxation processes ($T_v \approx 110–115$ °C, $E_a \approx 130–140$ kJ mol^{-1}, characteristic relaxation times on the order of tens of minutes at 180 °C). Beyond the primary vitrimeric response, the materials exhibited functional reprocessability: fractured samples could be successfully re-molded by hot pressing at elevated temperature, partially recovering mechanical integrity, in agreement with dynamic network rearrangement. In addition, shape memory and thermally induced shape recovery experiments demonstrated efficient programming and recovery at 90 °C, with high recovery ratios (>90%) maintained over multiple cycles. Surface wettability and stability studies highlighted differences between 4-arm and 6-arm architectures, while hydrolytic degradation experiments showed faster mass loss for 6-arm networks, particularly under alkaline conditions, consistent with higher solvent accessibility. Chemical recycling under alkaline hydrolysis enabled recovery of monomeric species, and proof-of-concept composite experiments demonstrated simultaneous recovery of both polymer matrix components and reinforcing carbon fibers. Overall, these results establish a fully bio-based vitrimer platform combining mechanical robustness, dynamic reprocessability, shape memory functionality, controlled degradability, and chemical recyclability.

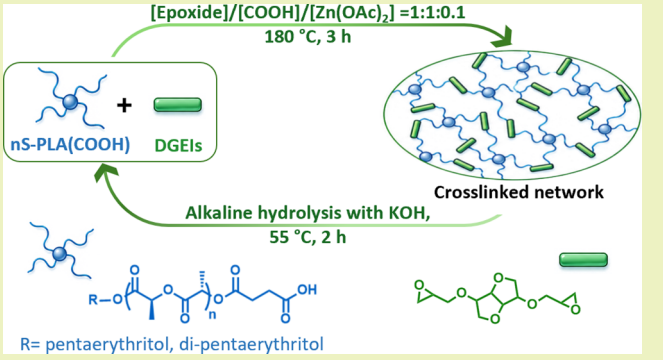

KEYWORDS: *sustainability, branched PLA, dynamic polymer networks, transesterification, circularity*

INTRODUCTION

The paradigm of circular economy, with the objective of reducing material consumption, material flows, and environmental pollution, is particularly challenging for the polymer sector. In fact, while collection, recycling, and reuse processes are well underway for thermoplastic polymers, at least in some industrial supply chains,[1] no eco-sustainable end-of-life solutions are currently available for thermosets. Thermosets are chemically cross-linked polymers, infusible, insoluble and with thermal and mechanical properties generally superior to thermoplastics. Thanks to their exceptional dimensional stability, they are widely used in many applications, accounting for about 18% of all polymers produced (over 65 million tons per year). Composite materials consisting of a thermosetting resin and a reinforcing fiber (mainly glass fiber or carbon fiber) are widely used in key industrial sectors, such as automotive, nautical, energy (wind turbines), and furniture (plastic laminates). Due to their chemical nature, these materials are intrinsically not recyclable. In addition, currently used thermosets are based on fossil, often toxic, feedstocks, such as diisocyanates, formaldehyde, and bisphenol A. Although recent research has been directed toward the synthesis of thermosets based on bio-renewable sources,[2−4] such as vegetable oil, lignin, sugar, itaconic acid, most of them are not recyclable due to the permanent crosslinked structure like the traditional thermosets. To address the above issue, a promising research approach has emerged in

Received: May 15, 2026
Revised: June 15, 2026
Accepted: June 16, 2026
Published: July 8, 2026

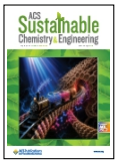

the last decade: the synthesis of polymer networks crosslinked with dynamic covalent bonds[5−9] (defined in the literature "covalent adaptable networks", CANs, or "dynamic polymer networks", or, in some cases, "vitrimers"[10]). These materials are designed to behave as the commonly available thermosets under service conditions, but, owing to the presence of weaker bonds in the crosslinks, they are potentially able to flow and thus to be reprocessed as thermoplastics under trigging stimuli (e. g. high temperature, catalyst or radiation). Several chemistries have been investigated for the development of CANs, such as olefin or dioxaborolane metathesis, imine chemistry, disulfide exchange, transamination of vinylogous urethanes, and siloxane/silyl ether reactions.[11−17] While promising, these methods often rely on costly or complex monomers and crosslinkers, limiting their scalability. A more practical route seems to adapt established chemistries like transesterification, using commercially available monomers. As a matter of fact, transesterification between carboxylic acids and hydroxyl groups in the presence of a catalyst was used by Leibler and coworkers in their pioneering work on vitrimers[18−20] and remains one of the most common strategies for the synthesis of CANs.[7,21−24] A further challenge for practical applications of vitrimers is the limited number of effective reprocessing cycles due to the downgrading of the material properties. This issue is especially critical for composite materials, which contain reinforcing fibers, whose recovery can be more valuable than that of the resin itself. An alternative approach involves the synthesis of thermosetting resins that can be subjected to chemical recycling at the end of their life, i.e., to a depolymerization process that leads to the recovery of the starting monomers.[25−28] We were interested in applying these concepts to develop recyclable thermosets based on poly(lactic acid) (PLA), the most commercially relevant bio-based polymer (with a current production capacity close to 1 million tons/year worldwide),[29,30] and an ideal candidate as a sustainable material, being simultaneously bio-renewable, biodegradable, and well suited for both mechanical and chemical recycling.[31−33] PLA-based polyester urethane vitrimers were previously synthesized from hydroxyl-terminated star-shaped oligomers of *rac*-lactide by crosslinking with methylene diphenyl diisocyanate.[34] These materials were able to relax stress at moderate temperatures in the presence of Sn(II) 2-ethylhexanoate, $Sn(Oct)_2$, showing healing capability via compression molding at 140 °C. Although their vitrimeric behavior was initially attributed to $Sn(Oct)_2$ catalyzed transesterifications, in a subsequent study the same group proposed that urethanes, not esters, were the dominant functional groups contributing to stress relaxation.[35] In this paper, we report the synthesis, the characterization and the chemical recycling of PLA-based vitrimers using a non-toxic and bio-based crosslinking agent, isosorbide diglycidyl ether (DGEIs), a sugar derived diepoxide which is considered as a green replacement for bisphenol A diglycidyl ether for the preparation of epoxy resins.[36,37]

EXPERIMENTAL SECTION

Experimental Details

All procedures involving air- and moisture-sensitive compounds were carried out under a nitrogen atmosphere in a Braun Labmaster glovebox or using Schlenk techniques. The glassware was dried in an oven at 120 °C overnight and subjected to vacuum-nitrogen cycles. Deuterated solvents were purchased from Aldrich. Methanol was dried over sodium and distilled under nitrogen. The technical-grade L-lactide used was Lumilact L, purchased from Total-Corbion, with a water content ≤0.03% w/w, and it was dried over P_2O_5 overnight. Similarly, the polyalcohols used were treated in the same manner. Isosorbide diglycidyl ether (DGEIs) was used as received from Specific Polymers. The material is defined by its epoxy equivalent weight (EEW) and consists of a distribution of monomeric and low-molecular-weight oligomeric species typically arising from the glycidylation process of isosorbide (see Scheme S1).[36] The same commercial batch was used throughout this study. Unless otherwise stated, all other chemicals were commercially available and used as received.

Synthesis of Star-Shaped PLA Hydroxyl End-Capped Prepolymers (ns-PLA(OH), $n = 4$ or 6)

Inside an MBraun glove box, anhydrous L-lactide, the alcohol initiator (either pentaerythritol or dipentaerythritol), and the $Sn(Oct)_2$ catalyst were weighed and sequentially introduced into a 100 mL two-neck round-bottom flask equipped with a magnetic stir bar. For the synthesis of the 4s-PLA(*OH*) prepolymers, the following amounts of reagents were typically used: L-lactide (15 g, 0.10 mol), pentaerythritol (1.2 g, 8.8 mmol), and $Sn(Oct)_2$ (14 mg, 3.4×10^{-5} mol). For the synthesis of the 6s-PLA(*OH*) prepolymers, L-lactide (15 g, 0.10 mol), dipentaerythritol (1.4 g, 5.5 mmol), and $Sn(Oct)_2$ (8.9 mg, 2.2×10^{-5} mol) were used. The reaction mixture was then removed from the glove box and placed in a preheated oil bath at 160 °C under stirring for 4 h. After completion of the reaction, the polymer was recovered by pouring the reaction mixture into hexane. The resulting white solid was collected by decantation and dried first under reduced pressure to remove residual solvent and then under high vacuum at 100 °C.[34]

4s-PLA(*OH*): ^{1}H-NMR (300 MHz, $CDCl_3$, 298 K) δ: 5.17 ppm (m, 1nH), 4.35 (q, $J = 6.9$ MHz, 1nH), 4.17 (br, 2nH), 1.57 (d, $J = 5.2$, 3nH), 1.48 (d, $J = 7.4$, 3nH). ^{13}C-NMR (75 MHz, $CDCl_3$, 298 K) δ: 175.27, 169.74, 69.14, 66.85, 62.53, 20.64, 16.78. 6s-PLA(*OH*): ^{1}H-NMR (600 MHz, $CDCl_3$, 298 K) δ: 5.16 (m, 1nH), 4.34 (q, $J = 7.4$ MHz, 1nH), 4.15 (br, 2H), 3.37 (br, 2nH), 1.57 (d, $J = 7.37$, 3nH), 1.48 (d, $J = 7.37$, 3nH). ^{13}C-NMR (100 MHz, $CDCl_3$, 298 K) δ: 174.69, 169.15, 68.56, 66.27, 62.43, 43.34, 20.06, 15,37.

Synthesis of Star-Shaped PLA Carboxyl End-Capped Prepolymers

Hydroxyl-terminated star-shaped PLA prepolymers were converted into carboxylic acid-terminated polymers through reaction of the terminal hydroxyl groups with succinic anhydride.[38] In a typical procedure, 15 g of either 4s-PLA(*OH*) or 6s-PLA(*OH*) were dissolved in 20 mL of 1,4-dioxane. Succinic anhydride was then added in an equimolar amount relative to the hydroxyl functionalities (3.3 g, 0.033 mol for 4s-PLA(*OH*); 3.2 g, 0.032 mol for 6s-PLA(*OH*)). After complete dissolution of the reagents, triethylamine (TEA, 0.075 g, 0.10 mL, 7.4×10^{-4} mol) and 4-dimethylaminopyridine (DMAP, 0.075 g, 6.1×10^{-4} mol), each corresponding to 0.5 wt-% relative to the polymer, were added as catalysts, and the reaction mixtures were stirred overnight at approximately 25 °C. For both the 4s-PLA(*COOH*) and 6s-PLA(*COOH*) syntheses, after completion of the reaction, the solvent was removed under reduced pressure, and the crude products were subsequently dried under high vacuum at 100 °C to remove residual solvent (see Table S1).

4s-PLA(*COOH*): ^{1}H-NMR (400 MHz, $CDCl_3$, 297 K): δ 5.18 (m, 4nH), 4.17 (br, 2nH), 2.68 (s, 4H), 1.59 (d, 3nH, $J = 6.6$ Hz). ^{13}C-NMR (100 MHz, $CDCl_3$, 297 K): δ 175.17, 171.58, 169.61, 69.01, 66.72, 62.29, 28.61, 20.49, 16.64. 6s-PLA(*COOH*): ^{1}H-NMR (400 MHz, $CDCl_3$, 297 K): δ 5.16 (m, 6nH), 4.34 (q, 1H, $J = 7.0$ Hz), 4.15 (br, 2nH), 3.34 (br, 2nH), 2.70 (s, 4H), 1.57 (d, 3nH, $J = 6.8$ Hz). ^{13}C-NMR (100 MHz, $CDCl_3$, 297K): δ 175.16, 171.58, 169.61, 69.01, 66.72, 62.87, 43.34, 28.62, 20.50, 16.64.

Crosslinking Reaction and Thermoset Preparation

The crosslinking reaction was initially explored by dissolving ns-PLA(*COOH*) and DGEIs in dichloromethane and $Zn(OAc)_2$ in

https://doi.org/10.1021/acssuschemeng.6c05601
ACS Sustain. Chem. Eng. 2026, 14, 12997−13012

methanol, then combining and sonicating the solutions for 30 min. The mixture was cast into a Teflon Petri dish and left to evaporate overnight at room temperature. It was then heated under nitrogen with a gradual temperature ramp from 25 to 180 °C. The sample was then kept isothermally at 180 °C for 3 h (see Table S2).

We subsequently verified that the same synthetic strategy and comparable material properties can be achieved using greener solvents (i.e. 2-methyl-tetrahydrofuran, or methyl lactate), as well as solvent minimized bulk conditions. In particular, samples for tensile test, reprocessing, stress-relaxation, SEM images, ATR-FTIR, scratch-healing, DMTA and TGA-isotherm analysis were prepared following the latter procedure, i.e. heating separately at 80 °C for 30 min ns-PLA(*COOH*) and a solution of $Zn(OAc)_2$ in ethanol (280 mg/mL). Once the prepolymer had melted, DGEIs and the $Zn(OAc)_2$ solution were gradually added with continuous stirring. When a homogeneous mixture was achieved, the formulation was poured into a silicone mold and cured in an oven at 180 °C for 3 h. Further details are reported in the SI.

Nuclear Magnetic Resonance

NMR spectra were recorded using either a Bruker Advance 300, 400 or 600 MHz Ascend 3 HD spectrometer. Chemical shifts (δ) are expressed as parts per million and coupling constants (*J*) in hertz. ^{1}H NMR spectra are referenced using the residual solvent peak at δ 7.26 for $CDCl_3$. ^{13}C NMR spectra are referenced using the residual solvent peak at δ 77.22 for $CDCl_3$.

Differential Scanning Calorimetry

DSC analysis was performed on a TA Q2000 (TA Instruments) or on TA Q20 (TA Instrument) according to the following program: equilibrate at –20 °C; ramp 10.00 °C min^{-1} to 250 °C; ramp 10.00 °C min^{-1} to –20 °C. The instrument was calibrated for temperature and enthalpy by a high-purity indium (156.60 °C, 28.45 J/g) standard.

Gel Permeation Chromatography

GPC was performed using an Agilent 1260 Infinity Series GPC equipped with a ResiPore 3 μm, 300 × 7.5 mm column, operating at a flow rate of 1.0 mL/min. Detection was achieved using both a UV (250 nm) and a refractive index (RI, PLGPC 220) detector. All measurements were conducted with THF or $CHCl_3$ as the eluent at a flow rate of 1.0 mL/min and a column temperature of 35 °C. Monodisperse poly(styrene) polymers were used as calibration standards.

Matrix-Assisted Laser Desorption/Ionization

MALDI mass spectra were acquired using a Bruker solariX XR Fourier transform ion cyclotron resonance (FT-ICR) mass spectrometer (Bruker Daltonik GmbH, Bremen, Germany) equipped with a 7 T refrigerated actively shielded superconducting magnet.

Rheological Analysis

Rheological testing was performed using a rotational rheometer (Mars, Thermofisher) with a 25-mm parallel-plate geometry. Isothermal time-sweep mode tests were carried out at constant strain amplitude (10%) and frequency (1 Hz) within 1 h at three selected temperatures of interest, namely 140, 165, 180 °C, based on information collected in previous experiments.

Dynamic Mechanical Analysis

Dynamic-mechanical thermal analysis (DMTA) was conducted using an Anton Paar MCR 702e Multi Drive Rheometer (Graz, Austria) in tensile configuration, testing specimen with 30 mm of length, 5 mm of width, and 1 mm thickness, with a frequency of 1Hz and a strain of 0.01%. The storage modulus (E') and the loss factor (tanδ) were measured as a function of temperature. To estimate the apparent cross-linking density (ν_c), also referred to as strand density, the storage modulus values in the rubbery plateau region (E'_R) were extracted from the graph at approximately 30 °C above the glass transition temperature. Eq 1 was employed to calculate ν_c. This equation is based on the statistical theory of rubber elasticity, serving as an approximation to model the system, and was thus utilized primarily for qualitatively comparing the crosslinking levels among the networks obtained.

$$\nu_c = \frac{E'_R}{3RT} \tag{1}$$

where ν_c is the number of moles of network chains per unit volume of the cured network, R is the gas constant, and T is the absolute temperature (T_g + 30 °C).

Stress Relaxation

Stress relaxation tests were carried out using a modular compact rheometer (MCR 702e MultiDrive, Anton Paar, Ganz, Austria) equipped with a parallel plate geometry (sample thickness 1.8 mm, diameter 8 mm). Samples were subjected to a constant strain of 0.5% (selected in the linear viscoelastic region) and the consequent stress level was monitored as a function of time. The storage modulus $G(t)$ was normalized by the initial modulus G_0, and the characteristic relaxation time τ was determined as the time necessary to relax $1/e$ of the initial G_0 value. The activation energy E_a was calculated for each material by using an Arrhenius-type eq 2.

$$\ln \tau = \frac{E_a}{RT} - \ln A \tag{2}$$

Where R is the gas constant, T is the absolute temperature, and A is the pre-exponential factor. From the Arrhenius relation, the temperature of topology freezing (T_v) was obtained as the temperature at which the material reaches a viscosity of 10^{12} Pa s. Using Maxwell's relation and E' determined from DMTA (assuming E' being relatively invariant in the rubbery state), τ* was determined to be around 10^5 s in our systems. The Arrhenius relationship was then extrapolated to the corresponding value of τ*, to determine T_v for each sample.

Maxwell kinetic model for the stress relaxation 3, and stretched exponential model according to Kohlrausch–Williams–Watts function 4.[39]

$$\frac{G(t)}{G_0} = Ae^{-\frac{t}{\tau}} \tag{3}$$

$$\frac{G(t)}{G_0} = Ae^{-\left(\frac{t}{\tau}\right)^{\alpha}} \tag{4}$$

Where τ is the relaxation time, α is the stretched exponential, $G(t)$ is the decay of the relaxation modulus at time t, E_0 is the relaxation modulus at the initial time.

The vitrification temperature can be defined as the temperature at which the material has a viscosity 10^6 Pa s. Therefore, it is possible to calculate T_v by following the Maxwell equation 5 and extrapolating the Arrhenius plot.

$$\eta = \frac{E'}{3} \times \tau^* \tag{5}$$

Where E' is the storage modulus calculated in the rubbery plateau in the DMTA analysis and τ* is the relaxation time at T_v.

Shape Memory Behavior

The shape memory measurements were carried out on flat rectangular specimens in tensile configuration, while other mechanical deformations were performed but just for qualitative assessment. The ability

https://doi.org/10.1021/acssuschemeng.6c05601
ACS Sustain. Chem. Eng. 2026, 14, 12997−13012

of the samples to recover their original shape, defined as strain recovery (R_r) is calculated as follows:

$$R_r = \frac{\varepsilon_l(N) - \varepsilon_r(N)}{\varepsilon_l(N) - \varepsilon_r(N-1)} \quad (6)$$

where $\varepsilon_r(N)$ and $\varepsilon_r(N-1)$ are the residual strains after the recovery step for two consecutive thermo-mechanical cycles.[40]

Tensile Testing

The mechanical properties of the synthesized networks were assessed under uniaxial tension. Dog-bone-shaped specimens were prepared, featuring a rectangular gauge section with an effective length of approximately 25 mm, a width of 4 mm, and a thickness of roughly 1 mm. Tensile stress-strain measurements were conducted at room temperature using an INSTRON universal testing machine (Ulm, Germany) with a constant crosshead velocity of 1 mm/min following the ISO 527-2-5A standard. The samples were stretched to failure to determine key parameters, including Young's modulus (E'), ultimate tensile strength (σ_b) and elongation at break (ε_b). The reprocessing was performed by placing the broken samples under a hot press (Heated plates hydraulic press P200T Collin Maitenbeth, Germany) for 60 min at 10 bar and 180 °C.

Scanning Electron Microscopy (SEM)

The morphology of the samples was investigated through SEM imaging, carried out with a Phenom XL instrument (Thermo Fisher Scientific, USA) at a voltage of 10 kV in low vacuum configuration to avoid metallizing the surface of the sample.

Water Contact Angle (WCA)

WCA testing was carried out at room temperature using an FTA 1000 instrument (First Ten Ångstroms, UK). A 4 μL drop of deionized water was dispensed onto the sample surface via an automatic liquid drop dosing system. Images of the droplet on the surface were acquired at various time intervals, ranging from the moment of contact (i.e., 0 s) to 1000 s.

Fourier-Transform Infrared in Attenuated Total Reflection Mode (FTIR-ATR)

FTIR-ATR spectroscopy was performed using a Thermofisher spectrophotometer equipped with an attenuated total reflectance (ATR) apparatus. The spectra were recorded in the range 4000–4500 cm^{-1} using the following parameters: 4 cm^{-1} resolution, 32 accumulations. The epoxy group conversion was measured following the peak centered at around 910 cm^{-1}. Data were recorded and processed using the software Omnic from Thermo Fisher Scientific.

Thermogravimetric Analysis

Thermogravimetric analysis (TGA) in thermal ramp was carried out using a TA Instruments Q500 instrument produced by TA Instruments (Waters/TA Instruments). Polymer samples were placed in platinum crucibles and analyzed from 20 to 700 °C under a nitrogen atmosphere with a flow rate of 40.0 mL/min. TGA in isotherm was performed with a Mettler Toledo TGA/SDTA 851e. Samples (20 mg) were inserted in alumina crucibles and heated at 180 °C for 3 h under an air flux of 50 mL/min.

Scratch Healing Assay

The scratch healing capability was assessed by either optical microscopy or SEM image at different time steps. A crack was created on the surface of 1 mm or 0.1 mm samples, respectively, then the samples were quickly heated, and the recovery of the samples was monitored over time.

Disintegrability at pH = 5 and pH = 9

Chemical degradation of the samples was carried out under two different environmental conditions, namely pH = 5 and pH = 9, respectively achieved using acetate buffer and borate buffer solutions. 100 mg of film samples (L = 30 mm; W = 5 mm; T = 200 μm) were poured into 20 ml of each buffer solution at 25 °C. The time-evolution of mass retention was then calculated via gravimetric measurements at predetermined time intervals, according to a well-defined protocol reported elsewhere.[41−43]

Depolymerization of Thermoset Samples

In a typical experiment, 200 mg of a thermoset film sample was mixed in a 20 mL vial with 2 equivalents of KOH, calculated with respect to the estimated number of ester bonds in the sample. Distilled water (8 mL) was added as solvent. The vial containing the mixture was placed in a preheated oil bath at 55 °C and maintained under these conditions for 2 h. After this period, the original solid film was fully solubilized, and ^{1}H NMR analysis confirmed complete depolymerization, yielding lactic acid, succinic acid, and the hydrolysis product derived from isosorbide diglycidyl ether. ^{1}H NMR (400 MHz, $CDCl_3$, 298 K): δ 4.38 (q, 1H, J = 7.32 Hz, CH), 2.71 (s, 4H, CH_2), 1.49 (d, 3H, J = 6.85 Hz, CH_3).

RESULTS AND DISCUSSION

Synthesis of Star-Shaped PLA Carboxyl End-Capped Prepolymers

Hydroxyl end-capped 4-arm and 6-arm star-shaped poly(L-lactic acid) oligomers (ns-PLA(OH), n = 4 or 6) were synthesized by ring-opening polymerization of L-lactide using $Sn(Oct)_2$ as the catalyst, and pentaerythritol or dipentaerythritol as the co-initiator (see Scheme 1).[34]

The obtained polymers were analyzed by NMR and GPC. Although GPC data calibrated against polystyrene standards may be unreliable for branched architectures, the number-average molecular weights (M_n) estimated by ^{1}H NMR, based on the integration of signals associated with the pentaerythritol or dipentaerythritol core and those of the lactide repeating units (see Figures S1 and S2), show good internal consistency. Therefore, these values can be considered reasonably accurate, at least for comparative purposes. For the 4-arm systems (4s-PLA(OH)), M_n values in the 1.8–2.2 kDa range correspond to an average arm length of approximately 3 lactide units. MALDI-TOF analysis (see Figure S5) supports this interpretation, revealing a single dominant distribution with 72 Da spacing (lactic acid units) and a unimodal profile, consistent with a relatively well-defined star architecture, albeit with moderate intramolecular dispersity in arm length. For the 6-arm systems (6s-PLA(OH)), M_n values extend toward higher values (≈2.8–3.1 kDa), corresponding to slightly longer average arm lengths. In this case, MALDI-TOF spectra display a broader main distribution with a dominant star-shaped polymer population centered at approximately 3.2 kDa, corresponding to an average of ≈3.5 lactide units per arm (see Figure S6). Representative results are summarized in Table 1, while full data are reported in the Supporting Information.

The chemical structure of the 4-arm and 6-arm star-shaped PLA oligomers with hydroxyl end-groups was modified introducing acid functionalities on the chain terminals in order to improve their reactivity with the cross-linking agent. The terminal hydroxyl functionalities of the ns-PLA(OH) samples were acidified by reaction with succinic anhydride at 25 °C in 1,4-

https://doi.org/10.1021/acssuschemeng.6c05601
ACS Sustain. Chem. Eng. 2026, 14, 12997−13012

Scheme 1. Synthesis of 4s-PLA(*OH*) and 6s-PLA(*OH*) Oligomers

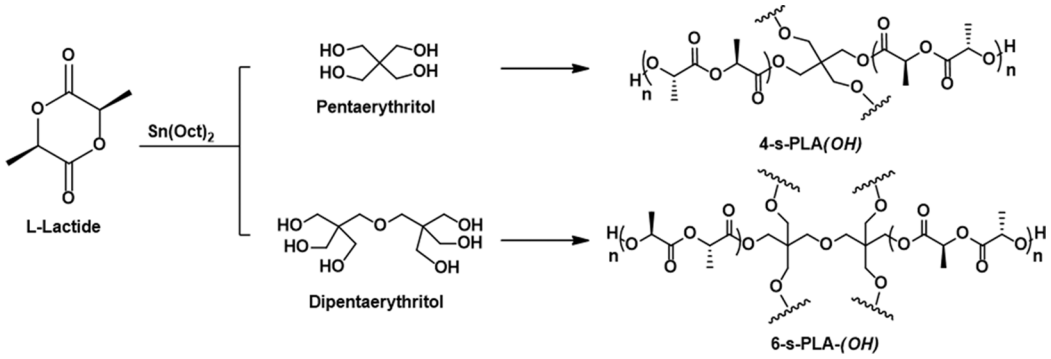

Table 1. Synthesis and Characterization of 4-Arm and 6-Arm Star-Shaped Low MW PLA Samples

	$M_{n(theo)}$ (kDa)	$M_{n(NMR)}$ (kDa)	$M_{n(GPC)}$[a] (kDa)	Đ[a]	$M_{n(MALDI)}$[b]	[LA]:[OH][c]	[LA]:[alcohol][d]
4s-PLA(*OH*)	1.8	1.9	2.2	1.3	1.8	3	13
6s-PLA(*OH*)	2.8	2.9	3.1	1.3	3.2	4	22

[a]Experimental M_n and M_w/M_n (Đ) values were determined by GPC analysis in THF vs. polystyrene standards (see Figures S7 and S8). [b]Estimated from MALDI-FT-ICR mass spectra. [c]Molar ratio between lactide units and chain ends determined from ^{1}H-NMR. [d]Molar ratio between lactide units and either pentaerythritol or dipentaerythritol incorporated into the polymer chain estimated from ^{1}H NMR.

dioxane solution in the presence of triethylamine (TEA) and 4-dimethylaminopyridine (DMAP) (see Scheme 2).[38]

The successful production of carboxyl acid-terminated star-PLA's (*n*s-PLA(*COOH*)) was confirmed by ^{1}H-NMR analysis, showing the appearance of the resonances of the methylene groups of the succinic acid moiety and the disappearance of the resonance due to the terminal C*H*-*OH* (see Figures S11 and S12). The degree of functionalization was determined by titration of the samples with a 0.1 M KOH solution in methanol. For the 4s sample, the theoretical carboxylic acid concentration was calculated to be 1.8 mmol g^{-1}, which closely matches the experimentally determined value of 1.8 mmol g^{-1}. For the 6s sample, the theoretical concentration is 1.7 mmol g^{-1}, whereas a slightly higher experimental value of 2.0 mmol g^{-1} was obtained (see Table S1).

Study of the Crosslinking Reaction with Isosorbide Diglycidyl Ether

The crosslinking reaction with isosorbide diglycidyl ether (DGEIs) was initially investigated using 4s-PLA(*COOH*) and $Zn(OAc)_2$ catalyst under different curing conditions (see Scheme 3 and Table S3).

Samples of 4s-PLA(*COOH*) were mixed with the proper amount of DGEIs in dichloromethane, and $Zn(OAc)_2$ was added as a solution in dry methanol. The solutions were poured into Teflon Petri dishes, casted at room temperature overnight, and then placed in an oven under a nitrogen atmosphere. A systematic screening of curing conditions (amount of catalyst, ratio between the epoxy functionalities of DGEIs and the carboxyl end-groups of the polymer, temperature and reaction time) was performed to evaluate the effect on network formation and final properties. The gel fractions of the resulting materials were measured in boiling chloroform. The main results, reported in Table S3, clearly show that lower catalyst loadings (2–5 mol%) lead to incomplete curing, as evidenced by significantly reduced gel fractions (58–87%), indicating an insufficient extent of network formation under otherwise identical conditions. Increasing the catalyst content to 10 mol% results in a substantial improvement in crosslinking efficiency, yielding gel fractions above 90% and significantly higher swelling resistance, consistent with the formation of a well-developed network. Additional variations in reaction time and temperature further confirm that full network formation requires sufficiently high catalytic activity, with 180 °C and 3 h providing optimal and reproducible curing conditions. Therefore, 10 mol% $Zn(OAc)_2$ was selected as the optimal compromise ensuring complete curing, high gel fraction, and mechanically robust networks, and this condition was used consistently throughout the study for all subsequent characterizations, including mechanical, thermal, and viscoelastic analyses.

The products obtained after the curing reaction, and, for comparison, the pre-curing reaction mixtures, were subjected to differential scanning calorimetry (DSC) analysis, confirming the above indication. In fact, while large exothermic peaks were observed for all the pre-curing mixtures, no exothermic peak was observed, e.g., for the material cured at 180 °C for 3 h (see Entry 3 of Table S3), confirming the formation of a completely crosslinked network (see Figures 1 and S15). On the contrary, exothermic peaks were observed, e.g., in the DSC of samples produced using a lower amount of $Zn(OAc)_2$ (see Entries 1 and 2 of Table S3 and Figure S16), indicating an incomplete curing reaction.

It is worth noting that no crystallization or melting transitions were observed either for the star-shaped PLA prepolymers (see Figure S17) or for the corresponding vitrimer networks. This behavior is attributed primarily to the very short PLA arm length, which prevents the formation of stable crystalline domains, while crosslinking further suppresses chain organization.

In response to the Editor's and Reviewers' recommendations regarding solvent sustainability,[44] we verified that the same

https://doi.org/10.1021/acssuschemeng.6c05601
ACS Sustain. Chem. Eng. 2026, 14, 12997−13012

Scheme 2. Acidification of Hydroxyl End-Groups of the *ns*-PLA(*OH*) Samples

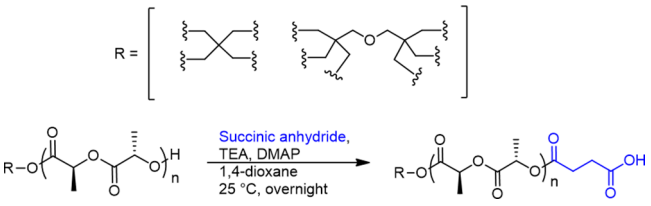

synthetic strategy can be successfully implemented using greener solvents, such as 2-methyltetrahydrofuran or methyl lactate (see Figure S18 and the SI for details), as well as solvent-minimized bulk curing conditions (see below, the Experimental Section, and Figure S19), without compromising the overall material performance.

The rheological behavior of the precursor mixtures for PLA-based thermosetting resins was investigated using a parallel-plate rheometer, providing direct insight into the temperature-controlled curing mechanism. Temperature-sweep experiments, as shown in Figure 2, revealed a sharp, exponential increase in viscosity above approximately 170 °C, identifying this range as the threshold for activation of the crosslinking reaction. Below this temperature, the system remained readily processable, whereas above it the rapid viscosity build-up reflected the onset of network formation. Isothermal time-sweep measurements further clarified how temperature governed both the kinetics and extent of curing. As shown in Figure 3A,B, at 140 °C, the absence of significant changes in the storage modulus, loss modulus, and complex viscosity confirmed that the system remained in a precursor, liquid-like state, with negligible network development. Raising the temperature to 165 °C (Figure 3C) initiated a gradual formation of a percolated network, as indicated by the progressive increase of complex viscosity (Figure 3A) and storage and loss moduli (Figure 3C) with the crossover of G' and G'' at 100 s, signaling the transition toward solid-like behavior. At 180 °C, as can be seen in Figure 3A,D, crosslinking proceeded rapidly and efficiently, leading to steep increases in storage modulus (G') and viscosity and resulting in a highly crosslinked network within a short time. These rheological observations were fully consistent with the gel fraction data, which showed a dramatic increase in insoluble content with temperature. While curing at 140 °C yielded only negligible gel formation and 165 °C led to partial network development, curing at 180 °C produced gel fractions exceeding 90% after 1 h (Tables 2 and S3), comparable to those obtained after prolonged curing. Collectively, these results demonstrated that curing temperature was the key parameter controlling network formation in this system and identified 180 °C as the optimal condition to achieve fast, efficient, and reproducible formation of robust PLA-based networks.

Similar experiments were carried out using a 6s-PLA(*COOH*) prepolymer, resulting in a comparable trend between the two systems (see the SI, Figures S20 and S21).

Physical Characterization of the PLA-DGEIs Thermosets

Based on the above studies, crosslinked film samples were prepared by curing formulations based on ns-PLA(*COOH*) prepolymers (n = 4 or 6) with an epoxide/(*COOH*)/$Zn(OAc)_2$ molar ratio of 1:1:0.1 at 180 °C for 3 h (see the Experimental Section for details). Table 2 summarizes the properties of two representative film samples. To evaluate the efficiency of the crosslinking reaction, ATR-FTIR spectra were collected before and after curing. As shown in Figure 4, a complete conversion of the epoxy groups of DGEIs is observed upon curing, as evidenced by the disappearance of the characteristic C–O stretching vibrations of the epoxy ring at 912 and 834 cm^{-1}. This result confirms the full consumption of epoxy functionalities and is consistent with previously reported PLA–epoxy vitrimer systems cured at 180 °C.[45−47] In the post-curing spectrum of the 4s sample, an increase in the intensity of the broad band centered at approximately 3500 cm^{-1} can be observed, attributed to O–H stretching vibrations arising from the formation of hydroxyl groups upon epoxy ring opening. Furthermore, new absorption bands appear at 1160 and 1630 cm^{-1}, which can be assigned to C–O–C (β-hydroxy ester) linkages and to carbonyl groups formed during the curing process, respectively. These results are in good agreement with the high gel fractions, higher than 95%, reported in Table 2 (see the Experimental Section for details).

Despite the very high gel fractions, the materials exhibit large swelling ratios in chloroform. This apparent discrepancy can be rationalized by considering the specific architecture of the PLA–DGEIs networks. While the high gel fraction confirms that most polymer chains are incorporated into a continuous network, it does not directly reflect the crosslink density. In the present systems, the crosslinking junctions are connected by relatively long and flexible PLA segments ($M_n \approx$ 1–3 kDa). Therefore, the network can accommodate significant solvent uptake without dissolution. This effect is further enhanced by the good affinity of chloroform for PLA, which promotes extensive swelling of the polymer chains. Accordingly, the observed behavior is consistent with loosely crosslinked networks containing long, flexible segments between junction points, where high gel fraction and high swelling can coexist. In addition, due to the polyester-based and vitrimeric nature of these materials, swelling experiments were performed in boiling chloroform to ensure that equilibrium conditions were reached within a reasonable timescale. At room temperature, solvent diffusion into the glassy PLA-rich domains can be kinetically hindered, potentially leading to an underestimation of solvent uptake. Under reflux conditions, complete solvent penetration is achieved, allowing the intrinsic network openness and chain flexibility to be more accurately probed. Therefore, the swelling data should be interpreted qualitatively as an indication of network architecture and segmental mobility, rather than used for quantitative estimation of M_c. The dynamic nature of the ester-based network may further contribute to solvent uptake by enabling local rearrangements without loss of overall network connectivity.

SEM analyses were performed on the fractured surfaces of the cured films to investigate the morphological features and the distribution of the catalytic species within the matrix. Figure S22 shows representative micrographs of the investigated samples, together with the corresponding EDX area spectra reported on the left. The analyzed materials include a reference sample, obtained by physical mixing of PLA with DGEIs in the absence of $Zn(OAc)_2$, as well as the crosslinked vitrimeric systems 4s and 6s. The EDX analysis of the 4s and 6s samples clearly confirms the presence of zinc, which appears to be homogeneously distributed throughout the polymer

https://doi.org/10.1021/acssuschemeng.6c05601
ACS Sustain. Chem. Eng. 2026, 14, 12997−13012

Scheme 3. Crosslinking Reaction of ns-PLA(*COOH*)

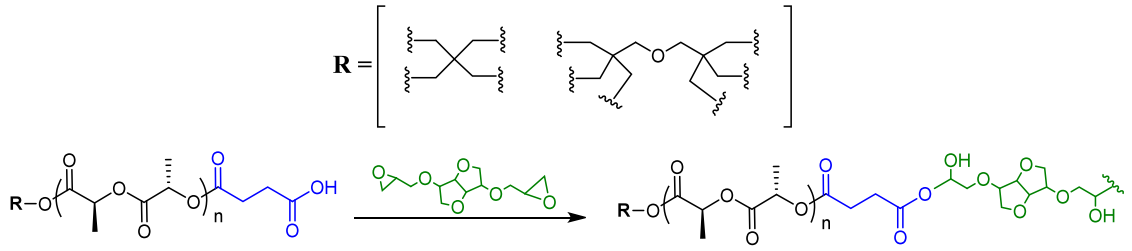

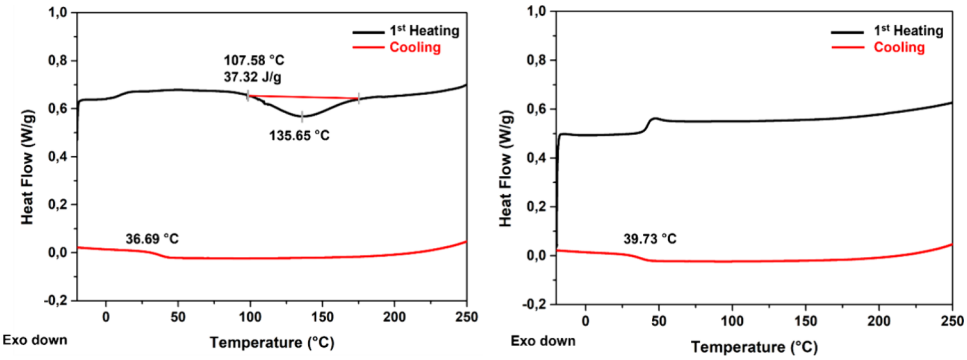

Figure 1. DSC analysis (exo down) of the pre-curing reaction mixture (left) and the cured product (right), corresponding to entry 3 in Table S3.

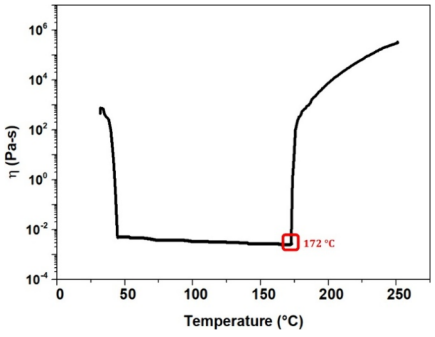

Figure 2. Temperature–sweep rheological analysis of a formulation prepared using 4s-PLA(*COOH*) as the prepolymer, with an epoxide/(*COOH*)/$Zn(OAc)_2$ molar ratio of 1:1:0.1

matrix, indicating an effective incorporation of the catalytic species within the crosslinked networks.

The thermomechanical properties of the thermoset samples were investigated by dynamic mechanical thermal analysis (DMTA) on rectangular bar specimens (30 mm × 5 mm × 1 mm) prepared according to the bulk-curing procedure described in the Experimental Section. The collected value of T_g, E' in the glassy state and rubbery state are reported in Table 3.

As illustrated in Figure 5, the rubbery modulus (E'_R) increased from the 4s sample to the 6s one, indicating the formation of more rigid networks. Numerous theories link rubbery modulus to the crosslinking density (ν_c) of the thermosetting network, suggesting that greater moduli are associated with higher crosslinking density. Table 3 presents the ν_c values for the two networks, demonstrating an enhanced ν_c for 6s samples, as expected for its increased functionalities. This result is in good agreement with the higher swelling ratio achieved by 4s with respect to 6s. The peak of the Tanδ, which can be attributed to the T_g of the polymer network, remains almost unchanged between the two samples, or even slightly higher in the case of 4s samples. This can be attributed to the high flexibility of the PLA arms, which mitigates the expected increase in network rigidity associated with higher crosslinking density. The relatively low T_g values of the vitrimer networks, compared to high-molecular-weight linear PLA, are consistent with the use of short star-shaped PLA oligomers ($M_n \approx 1$–3 kDa), as star/multi-arm PLA architectures are known to exhibit lower T_g values than their linear counterparts.[48,49] The presence of succinate- and β-hydroxy ester-containing linkages generated during epoxy–acid curing with DGEIs further contributes to segmental mobility. Notably, the more densely crosslinked 6s network displays a slightly lower T_g than the 4s analogue, indicating that network architecture and chain mobility play a more important role than crosslink density alone in determining the glass transition behavior.

Stress relaxation analyses were then performed in shear mode on disk-shaped specimens (8 mm diameter, 1 mm thickness, prepared as described in the Experimental Section) for each material in the linear viscoelastic regime, and the characteristic relaxation time τ* at each temperature was taken as the time required for the stress relaxation modulus to decay to $1/e$ of its initial value (G_0), as reported in Table S4. The relaxation plots reported in Figure 6 exhibit distinct relaxation profiles depending on the sample tested. The relaxation profile for the 4s formulation follows the typical behavior of vitrimeric systems, characterized by an initial slow stress reduction over time. The 6s formulation shows a significantly faster decay of the modulus (Cf. 6s τ* = 20 min vs 4s τ* = 37 min at 180°C), especially at the beginning of the test, possibly due to a higher initial density of exchangeable groups. These relaxation times

https://doi.org/10.1021/acssuschemeng.6c05601
ACS Sustain. Chem. Eng. 2026, 14, 12997−13012

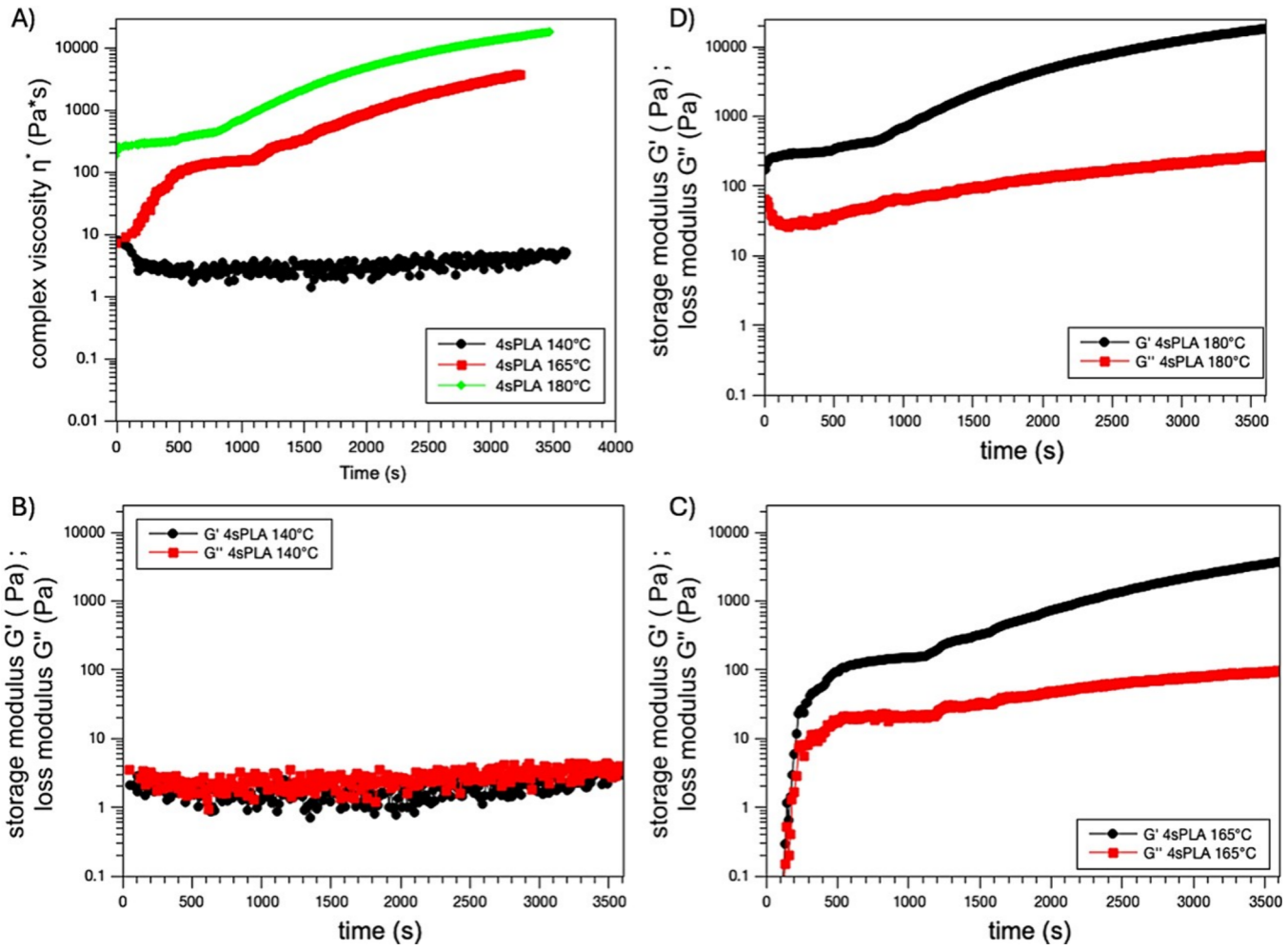

Figure 3. Evolution of complex viscosity as a function of time at three different temperatures (140, 165, and 180 °C) (A). Storage modulus (G') and loss modulus (G'') as a function of time at 140 °C (B), 165 °C (C), and 180 °C (D) for a 4s-PLA(COOH)/DGEIs/$Zn(OAc)_2$ mixture.

Table 2. Representative 4s-PLA(*COOH*) and 6s-PLA(*COOH*)/DGEI Crosslinked Samples

sample[a]	ns-PLA(*COOH*) acid (mmol/g)	gel fraction[b]	swelling[b]	thickness (μm)
4s	1.8	95%	1129 %	50
6s	2.0	96%	1005 %	50

[a]Film samples having ≈50 μm thickness were prepared using 0.5 g of prepolymer with [epoxide]:[COOH]:[$Zn(OAc)_2$] = 1:1:0.1, at 180 °C for 3 h. [b]Determined by extraction in boiling $CHCl_3$.

are consistent with the ones previously reported for related transesterification-based vitrimers.[50]

Typically, the Maxwell model is employed to fit stress relaxation data (refer to the method section); however, it did not yield a satisfactory fit for these samples (see Figure 6a,c), rendering it inapplicable for our analysis. Instead, we applied a stretched exponential fitting, which effectively captured the curves and provided a more accurate description of the stress-relaxation mechanism (as shown in Tables S4 and S5). The α values obtained illustrate the width of the distribution of relaxation times, with lower α values indicating more heterogeneous segment dynamics.

Notably, the stretching coefficient α demonstrated a strong temperature dependence in the 6s sample. At elevated temperatures, α values increased, suggesting that bond exchanges occur more freely, while lower temperatures resulted in a more complex relaxation process. Generally, an α value less than 1 may indicate a heterogeneous distribution of cross-links with varying strengths in these transient networks, or may reflect the presence of network defects such as dangling chains, trapped loops, and network strands.[39] In contrast, the α values for the 4s formulation remained relatively constant across all temperatures, indicating a simpler exchange reaction mechanism. This behavior is consistent with the higher intramolecular dispersity in arm length for 6s evidenced by MALDI-FT-ICR analysis, which is expected to generate a distribution of local environments and relaxation times within the network (see Figure S6).

https://doi.org/10.1021/acssuschemeng.6c05601
ACS Sustain. Chem. Eng. 2026, 14, 12997−13012

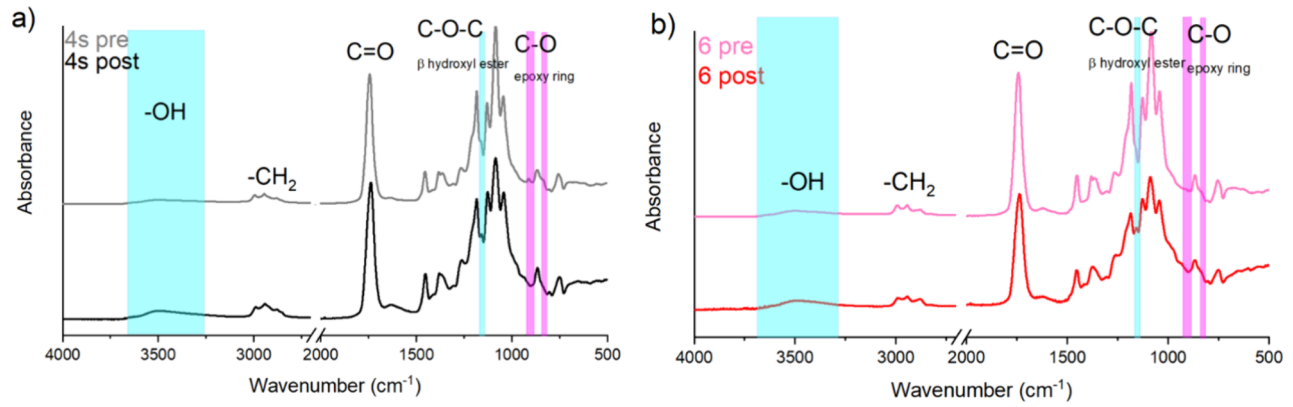

Figure 4. FTIR spectra of the 4s (a) and 6s (b) formulations before and after curing.

Table 3. DMTA-Derived Thermomechanical Parameters of the 4s and 6s Vitrimer Networks

samples	T_g (°C)	$E'_{glassy\_plateau}$ (GPa)	$E'_{rubbery\_plateau}$ (MPa)	ν_c [mol/dm^3]
4s	47	1.05	0.05	0.006
6s	43	3.88	0.29	0.034

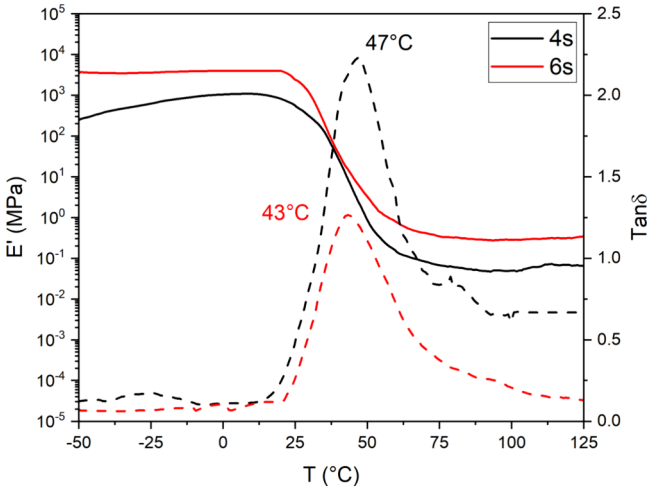

Figure 5. Storage modulus (E') and damping factor (Tan δ) of 4s and 6s samples as a function of temperature.

The activation energy (E_a) for both vitrimeric systems was determined using the Arrhenius plot (see Table 4 and Figure S23). The activation energy for the 6s sample was found to be 139 kJ/mol, which is higher than that of the 4s sample (133 kJ/mol). This is in good agreement with the higher cross-linking density of 6s evaluated by DMTA analysis. The E_a values achieved by these materials are in the same order of magnitude of other transesterification-based vitrimeric systems based on PLA previously reported in the literature (120–150 kJ/mol).[34]

The topological freezing temperature (vitrification temperature, T_v) was estimated by extrapolating the Arrhenius plot for the relaxation time according to the Maxwell model, as detailed in the Experimental Section. Both samples exhibit similar T_v, as expected for samples having similar T_g (Table 4). Although the present study does not allow direct experimental discrimination of the ester groups involved in the exchange reactions, literature on epoxy–acid vitrimers generally identifies the β-hydroxy ester moieties formed during epoxy/carboxylic acid curing as the most reactive sites toward transesterification.[47] In this context, the faster stress-relaxation behavior observed for the 6s network compared to the 4s analogue is consistent with a predominant contribution of these β-hydroxy ester groups to the exchange process. Indeed, while the two systems contain comparable amounts of PLA-derived ester groups, they differ in network architecture and in the relative abundance and local distribution of β-hydroxy ester linkages generated during curing.

Since both T_v values fall within the 110–113 °C range, temperatures below T_v can be exploited to activate shape memory behavior. To assess the shape memory capability of the vitrimeric systems, a series of experiments were performed on parallelepiped-shaped specimens. The programming step was carried out at 90 °C, after which the samples were mechanically deformed into different configurations, including stretching under an applied load, U-shaped bending, twisting, and folding. The temporary shape (TS) was then fixed by cooling the samples to room temperature. Upon reheating, the materials exhibited efficient shape recovery. The recovery ratio was evaluated after each cycle, and values up to 93% were retained even after five consecutive cycles (see Figure 7 and the video in the SI).

Dog-bone specimens for mechanical analysis were prepared following a solvent-minimized and environmentally conscious protocol: the 4s-PLA(*COOH*) and 6s-PLA(*COOH*) were first heated at 80 °C for 30 min, after which DGEIs and $Zn(OAc)_2$, previously dissolved in the minimum amount of ethanol required for complete solubilization of the salt, were added under continuous stirring. No additional organic solvents were used throughout the process. Once a homogeneous mixture was obtained, the formulations were cast into a silicone mold and thermally cured at 180 °C for 3 h (see Figure 8 and the Experimental Section).

The mechanical properties of the obtained materials (Virgin-V) and the recycled sample (R) were subsequently evaluated by tensile testing (see Figure 8 and Table 5). The virgin

https://doi.org/10.1021/acssuschemeng.6c05601
ACS Sustain. Chem. Eng. 2026, 14, 12997−13012

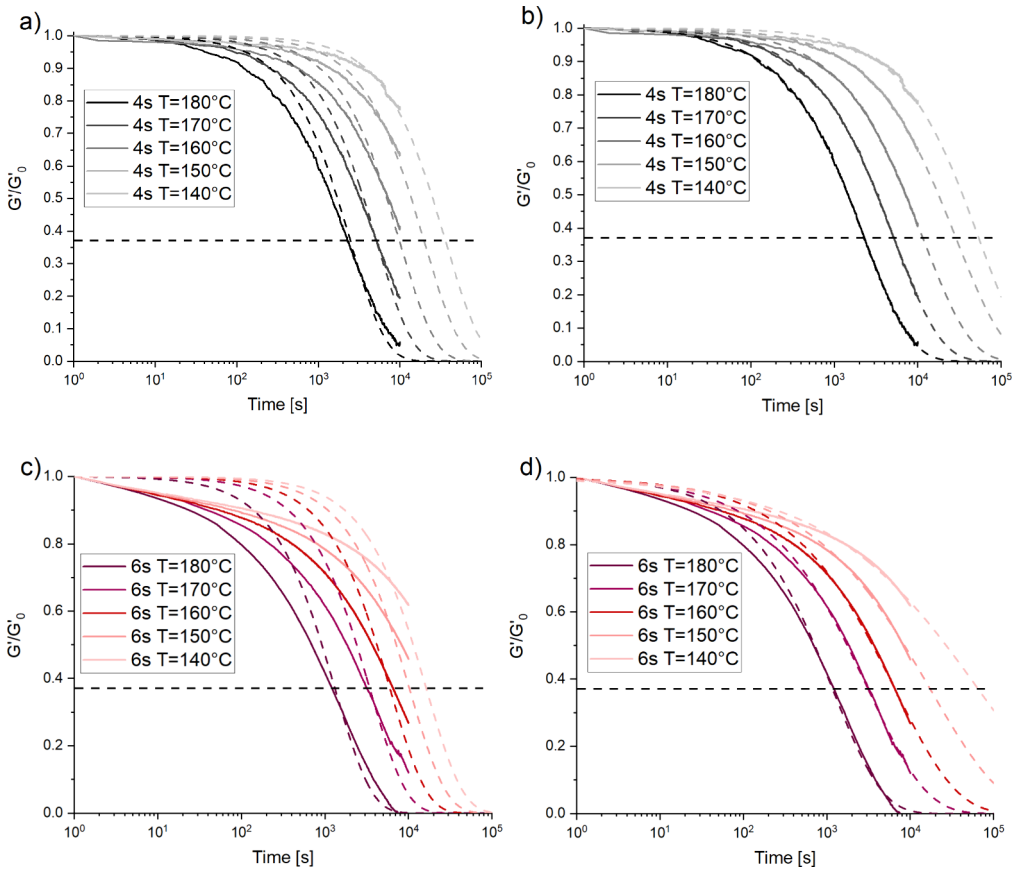

Figure 6. Stress–relaxation curves of 4s formulations fitted with (a) Maxwell model and (b) stretched exponential and 6s formulations fitted with (c) Maxwell model and (d) stretched exponential.

Table 4. Parameters Derived from the Arrhenius Plot

	T_v (°C)	E_a (kJ/mol)	R^2
4s	113	133	0.999
6s	110	139	0.991

materials exhibit excellent mechanical properties ($E \approx 2$ GPa, $\sigma_{max} \approx 40$ MPa, $\varepsilon_b \approx 2\%$), comparable or superior to those of linear PLA-epoxy vitrimer systems recently reported in the literature.[47] The observed mechanical profile, characterized by high stiffness combined with limited elongation at break, is consistent with the behavior expected for crosslinked PLA-based thermosets and suggests potential applicability in rigid to semi-rigid systems, such as dimensionally stable components, protective coatings, and matrices for recyclable fiber-reinforced composites (see below). After the first recycling step the mechanical properties of the samples were slightly reduced, which is quite common in vitrimer materials and can be attributed to two primary phenomena: (i) random chain scission, due to the hydrolysis of the PLA chains since the reprocessing was not conducted in an inert atmosphere[34,51] or (ii) polydispersity of chains length increase during the bonds exchange leading to a less uniform network formation with a consequent inefficient mechanical stress distribution.[31,52] Although some reduction in mechanical performance was observed after reprocessing, the recycled specimens remained self-supporting and mechanically robust, confirming the ability of the network to undergo thermally activated bond-exchange reactions and be reprocessed into new shapes. Further improvements in property retention may be achieved through optimization of the reprocessing conditions, including shorter residence times at elevated temperature, processing under inert atmosphere, and catalyst optimization to minimize undesired PLA degradation during thermal treatment.

Finally, the self-healing performance of the 4s material was evaluated by cutting a specimen and monitoring its healing behavior at 180 °C. The recovery process was followed at different time intervals using both optical microscopy and scanning electron microscopy (SEM) to assess the evolution of surface morphology and interfacial re-bonding (see Figures S24 and S25).

Surface Wettability and Hydrolytic Degradation of the PLA-DGEI Thermosets

The dynamic behavior of water contact angle (WCA) is shown in Figure 9 left, along with the corresponding digital images at 20, 250, and 1000 s shown in Figure 9 right. Water contact angles as a function of time provide insight into thermoset surface wettability and temporal stability under ambient conditions. From the WCA vs. time plot (Figure 9, left), it is evident that 4s exhibits higher initial WCA values (≈65°), maintaining higher values and exhibiting slower decay rates with respect to the 6s system. This behavior indicates a less wettable surface which could be attributed to a lower density of surface polar groups resulting from lower superficial hydroxyl functionality content.

https://doi.org/10.1021/acssuschemeng.6c05601
ACS Sustain. Chem. Eng. 2026, 14, 12997−13012

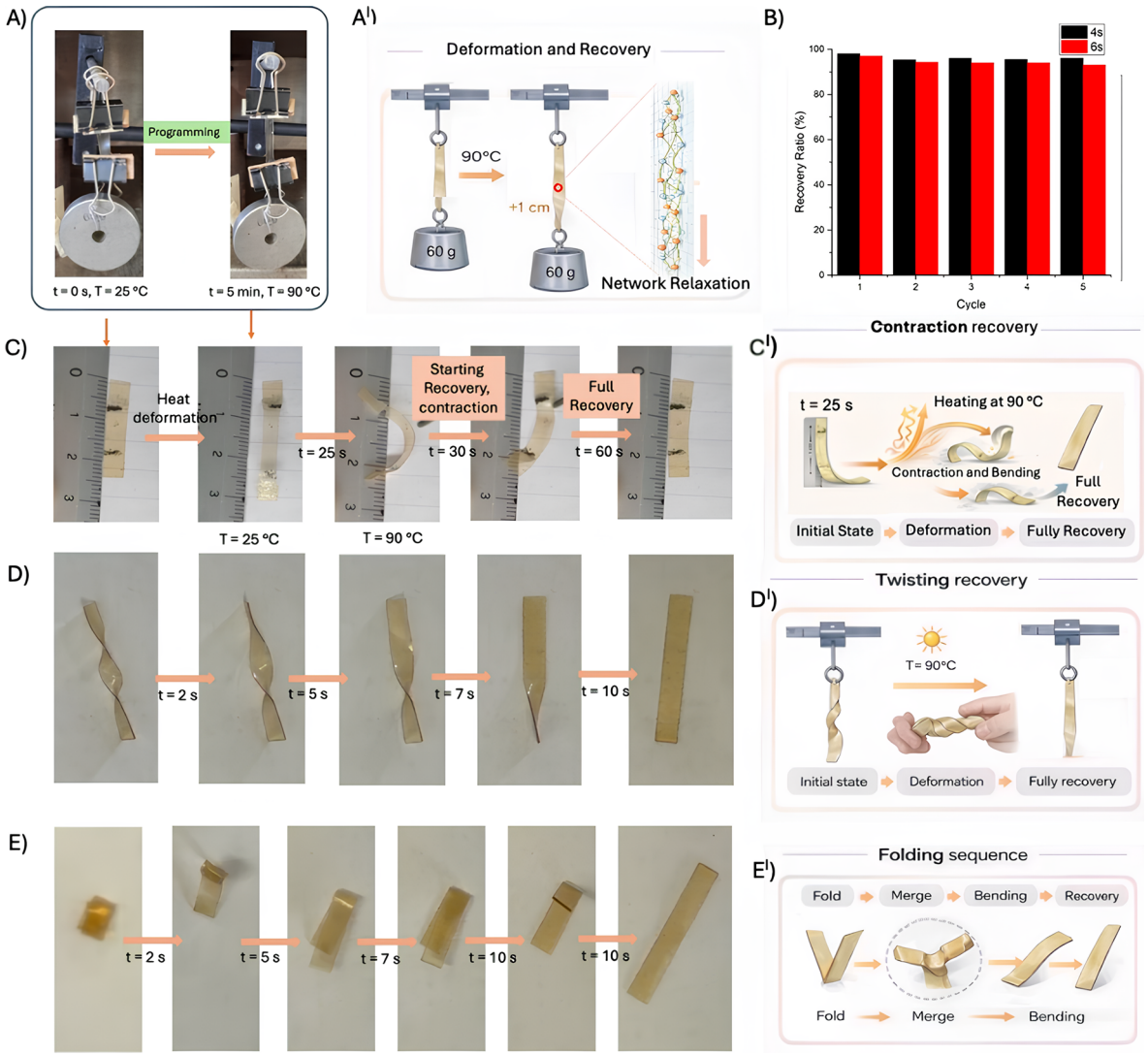

Figure 7. Shape memory behavior of a thin 4s film: (A) stretching under load; (B) recovery ratio as a function of the number of cycles; (C) U-shaped bending; (D) twisting; and (E) folding. The corresponding schematic representations are displayed in A′, C′, D′, and E′.

Accordingly, for the 4s sample, the droplets retain a near-hemispherical geometry over the entire time course, confirming more hydrophobic and temporally stable surfaces than 6s, which show more pronounced spreading and flattening of the droplet over time, indicating greater wettability.

The hydrolytic degradation of 4s and 6s thermosets was investigated under accelerated conditions at pH 5 and pH 9 at room temperature (≈25 °C). Over a 20-day period (Figure 10), the 6s-based vitrimer showed markedly higher degradation rates, particularly under alkaline conditions, where it lost nearly 50% of its mass, while the 4s counterpart retained approximately 90% of its initial mass. A similar, though less pronounced, trend was observed at pH 5, with the 6s system again degrading more rapidly.

This behavior can be rationalized by considering the different surface properties of the two networks. As discussed above, wettability measurements indicated that the 6s systems exhibit a higher affinity for water compared to their 4s counterparts. The enhanced surface wettability facilitates water uptake and diffusion into the material, thereby promoting hydrolytic cleavage of the ester bonds. In contrast, the lower wettability of the 4s networks limits water penetration, contributing to their greater resistance to degradation under identical conditions.

Macroscopic inspection after 20 days at pH 9 revealed a substantial loss of structural integrity in the 6s samples, which appeared delaminated and partially dissolved, whereas the 4s materials largely preserved their original shape. SEM analysis (see Figure S26) corroborated these observations and provided further insight into the degradation mechanisms. Prior to degradation, both systems exhibited smooth and homogeneous surfaces, indicative of effective curing. After hydrolytic treatment, surface erosion became evident in both materials; however, the 6s network underwent more severe damage, characterized by extensive porosity, matrix discontinuity, and deep internal fragmentation. In contrast, the 4s samples showed more limited erosion and retained a more coherent microstructure.

Overall, these results demonstrate that 6-arm PLA-based vitrimers are more susceptible to hydrolytic degradation, especially under alkaline conditions, where degradation extends

https://doi.org/10.1021/acssuschemeng.6c05601
ACS Sustain. Chem. Eng. 2026, 14, 12997−13012

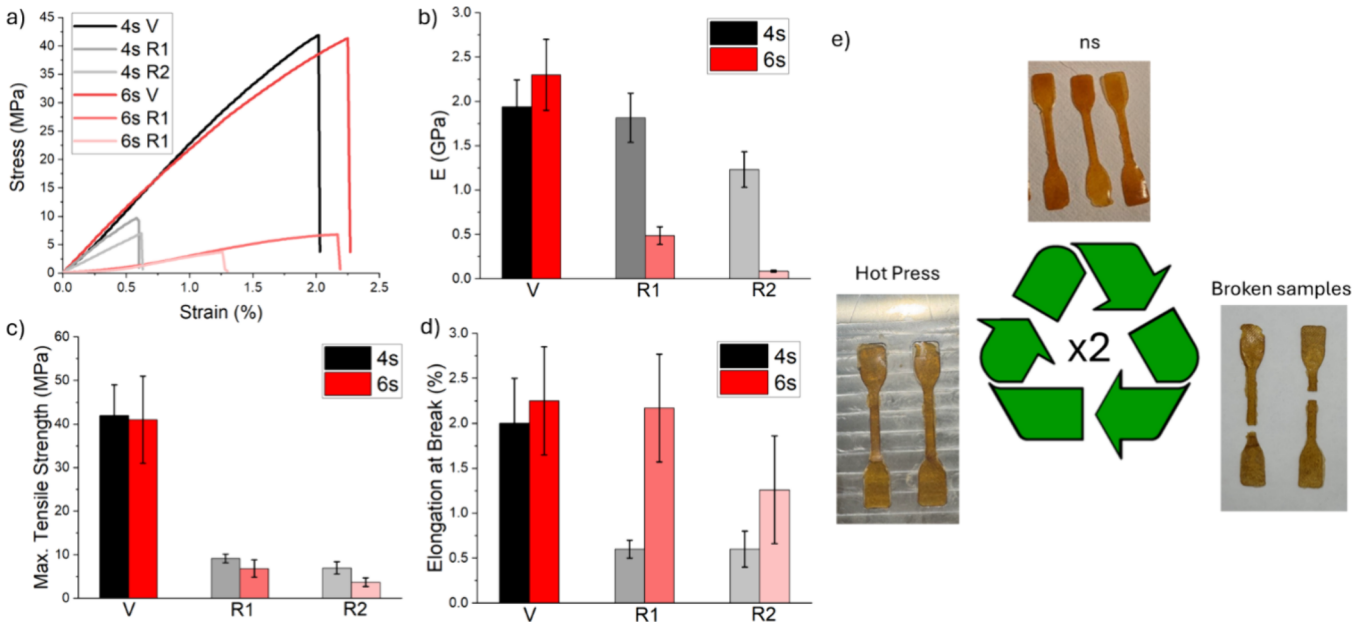

Figure 8. Tensile test comparison between 4s and 6s samples before and after the reprocessing cycles: (a) Stress–strain curves plots, (b) Young's modulus, (c) maximum tensile strength, (d) elongation at break, and (e) processing cycle scheme.

Table 5. Parameters Derived from the Stress–Strain Curve

	E (GPa)	σ_{max} (MPa)	ε_b (%)
4s V	1.94 ± 0.30	42.1 ± 7	2.1 ± 0.5
4s R1	1.82 ± 0.27	9.2 ± 1	0.6 ± 0.1
4s R2	1.23 ± 0.20	7.0 ± 1	0.6 ± 0.2
6s V	2.30 ± 0.40	41 ± 10	2.3 ± 0.6
6s R1	0.49 ± 0.11	6.8 ± 2	2.2 ± 0.6
6s R2	0.09 ± 0.02	3.7 ± 1	1.3 ± 0.5

beyond surface erosion into the bulk of the material. This behavior is consistent with their higher wettability and enhanced water accessibility. Conversely, the 4-arm systems exhibit reduced wettability and improved resistance to hydrolysis, maintaining greater structural cohesion and dimensional stability under the same conditions. These findings highlight a clear structure–property relationship, whereby the network architecture (i.e., arm functionality) governs surface wettability, which in turn controls water uptake and ultimately hydrolytic degradation kinetics. This provides a useful design parameter for tuning the balance between durability and degradability in PLA-based vitrimer systems. As these materials were specifically designed to combine vitrimeric behavior with hydrolytic degradability and chemical recyclability, a balance between service-life stability and end-of-life degradation must be achieved. The degradation experiments reported herein provide an initial assessment of network durability, whereas long-term aging under practical service conditions will be the subject of future studies.

Chemical Recycling of the PLA-Based Vitrimer Samples

We had recently reported the efficient alcoholysis of commercial PLLA samples, which produced alkyl lactates with high yield and selectivity by simply treating them in boiling methanol or ethanol in the presence of suitable (imidazo[1,5-*a*]pyrid-3-yl)phenolate Zn(II) catalysts.[53] We applied similar procedures to the PLA-based vitrimers: a crosslinked film sample was treated in boiling methanol in the presence of a Zn catalyst (see Scheme S2). The soluble fraction (≈10%) was extracted with $CHCl_3$, and after removal of all volatiles under reduced pressure, the residual products were analyzed by ^{1}H NMR, confirming the formation of methyl lactate and dimethyl succinate (Figure S27). A parallel experiment in boiling ethanol yielded ≈30% degradation, producing ethyl lactate and diethyl succinate (Figure S28; see the Supporting Information for procedure details). Given the modest efficiency of the Zn-catalyzed alcoholysis, we explored alkaline hydrolysis as an alternative recycling route. A vitrimer sample was treated with two equivalents of KOH (relative to the estimated number of ester linkages) in water at 55 °C. After 2 h, the sample was completely dissolved. The solution was then neutralized with HCl, extracted with chloroform, and analyzed by ^{1}H NMR, confirming the formation of lactic acid, succinic acid, and the hydrolysis product derived from isosorbide diglycidyl ether (Figures 11 and S29).

As highlighted in the introduction, a key goal for sustainable thermosets is the chemical recycling of composites, enabling recovery of both the resin and the reinforcing fiber, a process that is typically challenging.[27,54−58] To demonstrate this concept, a composite containing 55 wt% carbon fibers and 45 wt% of a 4s-PLA(COOH) / DGEIs / Zn(II) acetate resin mixture was prepared as described in the SI. After curing, the composite was subjected to alkaline hydrolysis under the same conditions used for the neat thermoset (Figure S30). The carbon fibers were successfully recovered, with their structural integrity preserved as can be observed in the SEM images in Figure S31, while analysis of the solution confirmed the recovery of lactic acid, succinic acid, and the hydrolysis product originating from isosorbide diglycidyl ether. These results provide a proof of principle for the chemical recycling of PLA-based vitrimer composites with simultaneous recovery of both resin-derived molecular species and reinforcing fibers. In this context,

https://doi.org/10.1021/acssuschemeng.6c05601
ACS Sustain. Chem. Eng. 2026, 14, 12997−13012

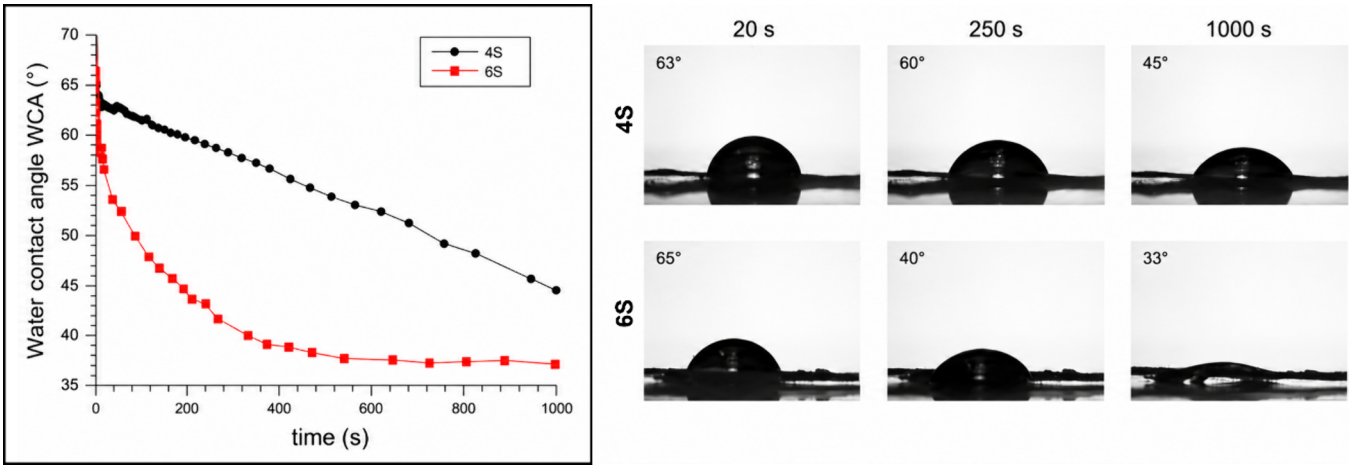

Figure 9. Water contact angle (WCA) evolution over time and droplet shape for 4s and 6s samples.

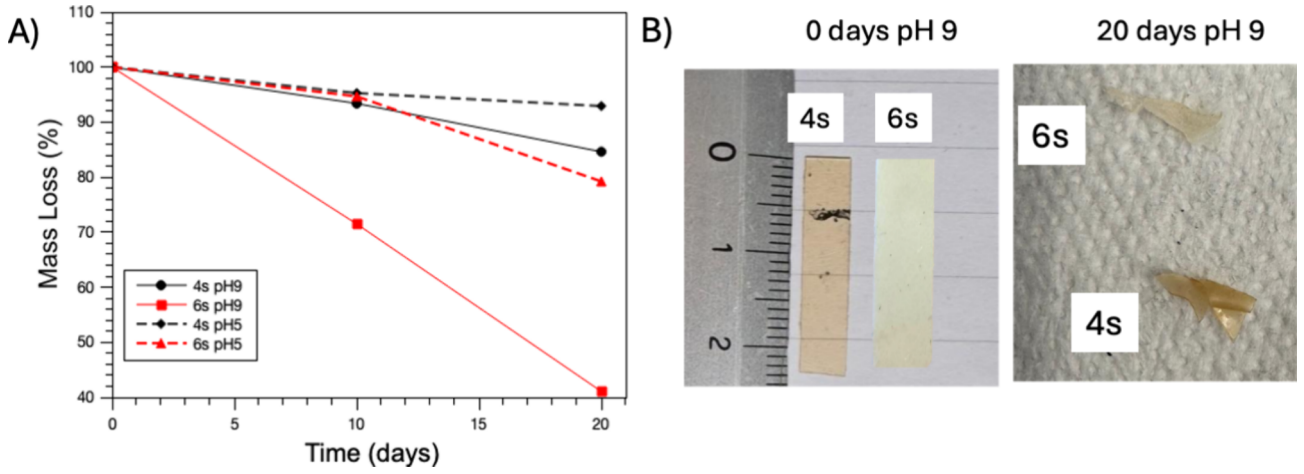

Figure 10. (A) Mass loss kinetics at pH = 9 and pH = 5 for a 4s (black curve) and a 6s (red curve) thermoset sample. (B) Visual comparison of resin morphology after degradation at pH 9.

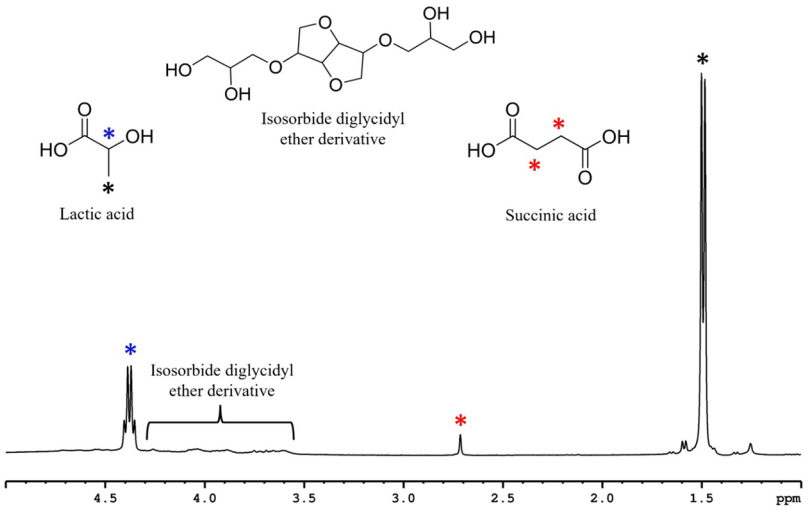

Figure 11. ^{1}H-NMR spectrum of products obtained from chemical recycling of a 4s-PLA(*COOH*)-based vitrimer sample by alkaline hydrolysis.

https://doi.org/10.1021/acssuschemeng.6c05601
ACS Sustain. Chem. Eng. 2026, 14, 12997−13012

the present study focuses on demonstrating the complete depolymerization of the network into its constitutive chemical building blocks, as confirmed by ^{1}H-NMR analysis of the crude hydrolysate. While isolation of individual monomers and repolymerization into oligomers or vitrimer networks was not pursued at this stage, the observed clean breakdown into the expected molecular species provides a solid basis for future investigations aimed at full material reconstitution and process-level circularity.

Preliminary Sustainability Assessment

This work presents a significant advancement in sustainable thermosetting polymers by seamlessly integrating renewable feedstocks, greener processing, and end-of-life circularity. Unlike conventional petroleum-based thermosets, these novel vitrimers are synthesized almost entirely from renewable biological sources, utilizing poly(lactic acid) (PLA) as the primary structural component and a bio-based isosorbide diglycidyl ether as a safe, green alternative to toxic bisphenol A (BPA) cross-linkers (see Table S6 for the renewable carbon content calculation). The manufacturing process further minimizes environmental impact by employing greener solvents alongside solvent-minimized bulk curing methods. Most importantly, the material directly addresses the global challenge of plastic waste through its inherent circularity. Thanks to dynamic chemical bonds, the vitrimer can be easily repaired, reshaped, and reprocessed using a hot press, which significantly extends its service life. At the end of its lifecycle, it overcomes the traditional recycling limitations of thermosets through a mild alkaline hydrolysis process that completely depolymerizes the material into its original building blocks. Remarkably, this chemical recycling method is also effective for carbon fiber-reinforced composites, successfully recovering both the reusable monomers and the structurally intact carbon fibers, offering a comprehensive and truly sustainable alternative to conventional, non-recyclable materials.

■ CONCLUSIONS

In this study, we have presented the design and characterization of fully biobased vitrimer networks derived from 4- and 6-arm star-shaped PLA oligomers, functionalized with carboxylic acid end-groups, and crosslinked with isosorbide diglycidyl ether. The optimized curing protocol produced homogeneous and robust thermoset networks with high gel fractions (>90%), demonstrating the effective formation of a stable, well-connected polymer architecture. Mechanical characterization confirmed that these networks combine notable stiffness and ductility, with Young's moduli in the range of 1.9–2.3 GPa and elongations at break of 2.1–2.3%, while dynamic mechanical analysis and stress relaxation studies revealed clear vitrimeric behavior, characterized by thermally activated bond exchange and Arrhenius-type relaxation kinetics. Consistent with these dynamic properties, the networks could be successfully reprocessed into new shapes through thermal treatment, although some reduction in mechanical performance was observed after the first recycling cycle, likely due to partial degradation of the PLA segments during processing. Surface wettability investigations highlighted that the 4-arm networks form more hydrophobic and temporally stable surfaces, whereas the 6-arm networks exhibit higher surface polarity and greater susceptibility to hydrolytic degradation, particularly under alkaline conditions. These findings indicate that structural design at the molecular level can finely tune both surface properties and degradation behavior, offering a handle for tailoring materials to specific applications. The recyclability of these PLA–DGEIs vitrimers was successfully demonstrated through alkaline hydrolysis under mild conditions, enabling efficient depolymerization of the network into its constitutive molecular species, including lactic acid, succinic acid, and isosorbide-derived fragments, as confirmed by ^{1}H NMR analysis of the crude reaction mixture. Remarkably, proof-of-concept experiments on carbon fiber-reinforced composites further showed that both the polymer matrix components and the reinforcing fibers can be recovered under the same conditions, highlighting the potential of these systems for the development of circular composite materials. Taken together, these results demonstrate the promise of PLA–DGEIs vitrimers as sustainable alternative thermosets. Beyond vitrimeric reprocessability, the possibility to chemically depolymerize the network and recover both resin-derived products and reinforcing fibers highlights the potential of these materials as matrices for future circular composite applications. By integrating biobased feedstocks with tunable dynamic behavior, controlled degradability, and easy chemical recyclability, these materials establish a versatile platform for the development of circular polymer technologies. Future work will be devoted to the fabrication of composite materials, comprehensive evaluation of their mechanical and thermal performance, further optimization of reprocessing conditions, and the establishment of efficient recycling protocols for both fibers and resin matrices, ultimately enabling the realization of high-performance, eco-friendly composites where sustainability, functionality, and recyclability are fully integrated.

■ ASSOCIATED CONTENT

Supporting Information

The Supporting Information is available free of charge at https://pubs.acs.org/doi/10.1021/acssuschemeng.6c05601.

^{1}H and ^{13}C NMR spectra for ns-PLA(*OH*) and ns-PLA(*COOH*) characterization; FT-IR characterization, GPC and MALDI-FT-ICR of the PLA prepolymers; Supplementary thermal, mechanical, and morphological analyses (DSC, DMTA, SEM, TGA, Arrhenius plot); rheology temperature and time sweep tests of the 6s system; chemical recycling reaction; ^{1}H NMR of alcholysis products; photographs of depolymerization tests; SEM images of carbon fibers before and after recycling; data on the acidity of functionalized PLA and curing process optimization; experimental data for gel fraction and swelling tests; optical microscopy images for healing; renewable carbon content assessment (DOCX)

Video showing a shape-memory recovery experiment (MP4)

■ AUTHOR INFORMATION

Corresponding Authors

Roberto Scaffaro – *Dipartimento di Ingegneria, Università degli Studi di Palermo, Viale delle Scienze, 90128 Palermo, PA, Italy*; orcid.org/0000-0002-4830-0374; Email: roberto.scaffaro@unipa.it

Claudio Pellecchia – *Dipartimento di Chimica e Biologia "A. Zambelli", Università degli Studi di Salerno, via Giovanni*

https://doi.org/10.1021/acssuschemeng.6c05601
ACS Sustain. Chem. Eng. 2026, 14, 12997−13012

Paolo II 132, 84084 Fisciano, SA, Italy; orcid.org/0000-0003-4358-1776; Email: cpellecchia@unisa.it

Authors

Licia Gaeta – *Dipartimento di Chimica e Biologia "A. Zambelli", Università degli Studi di Salerno, via Giovanni Paolo II 132, 84084 Fisciano, SA, Italy; Dipartimento di Ingegneria Industriale, Università degli Studi di Padova, via Gradenigo, 6/a, 35131 Padova, PD, Italy*

Michele Gammino – *Dipartimento di Ingegneria, Università degli Studi di Palermo, Viale delle Scienze, 90128 Palermo, PA, Italy*

Camilla Noè – *Dipartimento di Scienza Applicata e Tecnologia, Politecnico di Torino, Corso Duca degli Abruzzi 24, 10129 Torino, Italy;* orcid.org/0000-0001-8982-0299

Maria Gentile – *Dipartimento di Chimica e Biologia "A. Zambelli", Università degli Studi di Salerno, via Giovanni Paolo II 132, 84084 Fisciano, SA, Italy; Dipartimento di Ingegneria Industriale, Università degli Studi di Padova, via Gradenigo, 6/a, 35131 Padova, PD, Italy*

Complete contact information is available at: https://pubs.acs.org/doi/10.1021/acssuschemeng.6c05601

Author Contributions

The manuscript was written through the contributions of all authors. All authors have approved the final version of the manuscript. L.G.: Experimental investigation, data curation, writing—original draft. M.G.: Experimental investigation, data curation, writing—original draft. C.N.: Experimental investigation, experimental supervision, writing—review and editing. M.G.: Experimental investigation, data curation. R.S.: Conceptualization, experimental supervision, writing—review and editing. C.P.: Conceptualization, experimental supervision, writing—review and editing.

Funding

This study was carried out within the PRIN 2022-PNRR P2022K9XN3 "New recyclable thermosetting and elastomeric polymeric materials based on bio-renewable feedstocks", CUP D53D23017130001.

Notes

The authors declare no competing financial interest.

■ ACKNOWLEDGMENTS

The authors thank Dr. Annalisa Pace for the preliminary studies carried out during her Master's internship and Dr. Joseph N. A. Tagoe for performing preliminary mechanical tests. They also thank Dr. Patrizia Oliva for technical assistance with NMR experiments, Dr. Mariagrazia Napoli for GPC measurements, Dr. Ivano Immediata for technical assistance with TGA and DSC experiments, and Dr. Patrizia Iannece for the MALDI-FT-ICR mass spectra measurements.

■ REFERENCES

(1) European Academies Science Advisory Council (EASAC) *Packaging Plastics in the Circular Economy*; EASAC Policy Report 39, **2020**. https://easac.eu/fileadmin/PDF_s/reports_statements/Plastics/EASAC_Plastics_complete_Web_PDF.pdf (accessed Dec 10, 2025).

(2) Ma, S.; Li, T.; Liu, X.; Zhu, J. Research Progress on Bio-based Thermosetting Resins. *Polym. Int.* **2016**, *65* (2), 164–173.

(3) Kumar, S.; Samal, S. K.; Mohanty, S.; Nayak, S. K. Recent Development of Biobased Epoxy Resins: A Review. *Polym.-Plast. Technol. Eng.* **2018**, *57* (3), 133–155.

(4) Veith, C.; Diot-Néant, F.; Miller, S. A.; Allais, F. Synthesis and Polymerization of Bio-Based Acrylates: A Review. *Polym. Chem.* **2020**, *11* (47), 7452–7470.

(5) Van Zee, N. J.; Nicolaÿ, R. Vitrimers: Permanently Crosslinked Polymers with Dynamic Network Topology. *Prog. Polym. Sci.* **2020**, *104*, 101233.

(6) Porath, L.; Soman, B.; Jing, B. B.; Evans, C. M. Vitrimers: Using Dynamic Associative Bonds to Control Viscoelasticity, Assembly, and Functionality in Polymer Networks. *ACS Macro Lett.* **2022**, *11* (4), 475–483.

(7) Lucherelli, M. A.; Duval, A.; Avérous, L. Biobased Vitrimers: Towards Sustainable and Adaptable Performing Polymer Materials. *Prog. Polym. Sci.* **2022**, *127*, 101515.

(8) Zhao, X.-L.; Tian, P.-X.; Li, Y.-D.; Zeng, J.-B. Biobased Covalent Adaptable Networks: Towards Better Sustainability of Thermosets. *Green Chem.* **2022**, *24* (11), 4363–4387.

(9) Vidil, T.; Llevot, A. Fully Biobased Vitrimers: Future Direction toward Sustainable Cross-Linked Polymers. *Macromol. Chem. Phys.* **2022**, *223* (13), 2100494.

(10) Montarnal, D.; Capelot, M.; Tournilhac, F.; Leibler, L. Silica-Like Malleable Materials from Permanent Organic Networks. *Science* **2011**, *334* (6058), 965–968.

(11) Liang, K.; Zhang, G.; Zhao, J.; Shi, L.; Cheng, J.; Zhang, J. Malleable, Recyclable, and Robust Poly (Amide–Imine) Vitrimers Prepared through a Green Polymerization Process. *ACS Sustainable Chem. Eng.* **2021**, *9* (16), 5673–5683.

(12) Lu, Y.-X.; Tournilhac, F.; Leibler, L.; Guan, Z. Making Insoluble Polymer Networks Malleable via Olefin Metathesis. *J. Am. Chem. Soc.* **2012**, *134* (20), 8424–8427.

(13) Wu, Y.; Yang, Y.; Qian, X.; Chen, Q.; Wei, Y.; Ji, Y. Liquid-Crystalline Soft Actuators with Switchable Thermal Reprogrammability. *Angew. Chem., Int. Ed.* **2020**, *132* (12), 4808–4814.

(14) Ma, Y.; Jiang, X.; Shi, Z.; Berrocal, J. A.; Weder, C. Closed-Loop Recycling of Vinylogous Urethane Vitrimers. *Angew. Chem., Int. Ed.* **2023**, *62* (36), e202306188.

(15) Luo, C.; Wang, W.; Yang, W.; Liu, X.; Lin, J.; Zhang, L.; He, S. High-Strength and Multi-Recyclable Epoxy Vitrimer Containing Dual-Dynamic Covalent Bonds Based on the Disulfide and Imine Bond Metathesis. *ACS Sustainable Chem. Eng.* **2023**, *11* (39), 14591–14600.

(16) Gosecki, M.; Gosecka, M. Boronic Acid Esters and Anhydrates as Dynamic Cross-Links in Vitrimers. *Polymers* **2022**, *14* (4), 842.

(17) Chen, X.; Dam, M. A.; Ono, K.; Mal, A.; Shen, H.; Nutt, S. R.; Sheran, K.; Wudl, F. A Thermally Re-Mendable Cross-Linked Polymeric Material. *Science* **2002**, *295* (5560), 1698–1702.

(18) Capelot, M.; Montarnal, D.; Tournilhac, F.; Leibler, L. Metal-Catalyzed Transesterification for Healing and Assembling of Thermosets. *J. Am. Chem. Soc.* **2012**, *134* (18), 7664–7667.

(19) Demongeot, A.; Groote, R.; Goossens, H.; Hoeks, T.; Tournilhac, F.; Leibler, L. Cross-Linking of Poly(Butylene Terephthalate) by Reactive Extrusion Using Zn(II) Epoxy-Vitrimer Chemistry. *Macromolecules* **2017**, *50* (16), 6117–6127.

(20) Denissen, W.; Rivero, G.; Nicolaÿ, R.; Leibler, L.; Winne, J. M.; Du Prez, F. E. Vinylogous Urethane Vitrimers. *Adv. Funct. Mater.* **2015**, *25* (16), 2451–2457.

(21) Concilio, M.; Sulley, G. S.; Vidal, F.; Brown, S.; Williams, C. K. Precise Carboxylic Acid-Functionalized Polyesters in Reprocessable Vitrimers. *J. Am. Chem. Soc.* **2025**, *147* (8), 6492–6502.

(22) McBride, M. K.; Worrell, B. T.; Brown, T.; Cox, L. M.; Sowan, N.; Wang, C.; Podgorski, M.; Martinez, A. M.; Bowman, C. N. Enabling Applications of Covalent Adaptable Networks. *Annu. Rev. Chem. Biomol. Eng.* **2019**, *10* (1), 175–198.

(23) Kloxin, C. J.; Bowman, C. N. Covalent Adaptable Networks: Smart, Reconfigurable and Responsive Network Systems. *Chem. Soc. Rev.* **2013**, *42* (17), 7161–7173.
(24) Zhang, V.; Kang, B.; Accardo, J. V.; Kalow, J. A. Structure–Reactivity–Property Relationships in Covalent Adaptable Networks. *J. Am. Chem. Soc.* **2022**, *144* (49), 22358–22377.
(25) Scaffaro, R.; Di Bartolo, A.; Dintcheva, N. T. Matrix and Filler Recycling of Carbon and Glass Fiber-Reinforced Polymer Composites: A Review. *Polymers* **2021**, *13* (21), 3817.
(26) Zhang, H.; Su, Z.; Wang, X. Starch-Based Rehealable and Degradable Bioplastic Enabled by Dynamic Imine Chemistry. *ACS Sustainable Chem. Eng.* **2022**, *10* (26), 8650–8657.
(27) Fortman, D. J.; Brutman, J. P.; De Hoe, G. X.; Snyder, R. L.; Dichtel, W. R.; Hillmyer, M. A. Approaches to Sustainable and Continually Recyclable Cross-Linked Polymers. *ACS Sustainable Chem. Eng.* **2018**, *6* (9), 11145–11159.
(28) Yue, L.; Su, Y.; Li, M.; Yu, L.; Montgomery, S. M.; Sun, X.; Finn, M. G.; Gutekunst, W. R.; Ramprasad, R.; Qi, H. J. One-Pot Synthesis of Depolymerizable δ -Lactone Based Vitrimers. *Adv. Mater.* **2023**, *35* (29), 2300954.
(29) Rezvani Ghomi, E. R.; Khosravi, F.; Saedi Ardahaei, A. S.; Dai, Y.; Neisiany, R. E.; Foroughi, F.; Wu, M.; Das, O.; Ramakrishna, S. The Life Cycle Assessment for Polylactic Acid (PLA) to Make It a Low-Carbon Material. *Polymers* **2021**, *13* (11), 1854.
(30) Taib, N.-A. A. B.; Rahman, M. R.; Huda, D.; Kuok, K. K.; Hamdan, S.; Bakri, M. K. B.; Julaihi, M. R. M. B.; Khan, A. A Review on Poly Lactic Acid (PLA) as a Biodegradable Polymer. *Polym. Bull.* **2023**, *80* (2), 1179–1213.
(31) Shi, C.; Quinn, E. C.; Diment, W. T.; Chen, E. Y.-X. Recyclable and (Bio)Degradable Polyesters in a Circular Plastics Economy. *Chem. Rev.* **2024**, *124* (7), 4393–4478.
(32) Pretula, J.; Slomkowski, S.; Penczek, S. Polylactides—Methods of Synthesis and Characterization. *Adv. Drug Deliv. Rev.* **2016**, *107*, 3–16.
(33) McGuire, T. M.; Buchard, A.; Williams, C. Chemical Recycling of Commercial Poly(L -Lactic Acid) to L -Lactide Using a High-Performance Sn(II)/Alcohol Catalyst System. *J. Am. Chem. Soc.* **2023**, *145* (36), 19840–19848.
(34) Brutman, J. P.; Delgado, P. A.; Hillmyer, M. A. Polylactide Vitrimers. *ACS Macro Lett.* **2014**, *3* (7), 607–610.
(35) Brutman, J. P.; Fortman, D. J.; De Hoe, G. X.; Dichtel, W. R.; Hillmyer, M. A. Mechanistic Study of Stress Relaxation in Urethane-Containing Polymer Networks. *J. Phys. Chem. B* **2019**, *123* (6), 1432–1441.
(36) Hong, J.; Radojčić, D.; Ionescu, M.; Petrović, Z. S.; Eastwood, E. Advanced Materials from Corn: Isosorbide-Based Epoxy Resins. *Polym. Chem.* **2014**, *5* (18), 5360–5368.
(37) Ma, Z.; Wang, Y.; Zhu, J.; Yu, J.; Hu, Z. Bio-based Epoxy Vitrimers: Reprocessibility, Controllable Shape Memory, and Degradability. *J. Polym. Sci., Part A Polym. Chem.* **2017**, *55* (10), 1790–1799.
(38) Lee, S.-H.; Hyun Kim, S.; Han, Y.-K.; Kim, Y. H. Synthesis and Degradation of End-Group-Functionalized Polylactide. *J. Polym. Sci., Part A Polym. Chem.* **2001**, *39* (7), 973–985.
(39) Lorenz, N.; Dyer, W. E.; Kumru, B. Exploring the Cure State Dependence of Relaxation and the Vitrimer Transition Phenomena of a Disulfide-Based Epoxy Vitrimer. *J. Polym. Sci.* **2025**, *63* (18), 3739–3751.
(40) Cosola, A.; Sangermano, M.; Terenziani, D.; Conti, R.; Messori, M.; Grützmacher, H.; Pirri, C. F.; Chiappone, A. DLP 3D – Printing of Shape Memory Polymers Stabilized by Thermoreversible Hydrogen Bonding Interactions. *Appl. Mater. Today* **2021**, *23*, 101060.
(41) Scaffaro, R.; Maio, A.; Gulino, E. F.; Pitarresi, G. Lignocellulosic Fillers and Graphene Nanoplatelets as Hybrid Reinforcement for Polylactic Acid: Effect on Mechanical Properties and Degradability. *Compos. Sci. Technol.* **2020**, *190*, 108008.
(42) Scaffaro, R.; Maio, A.; Gulino, E. F. Hydrolytic Degradation of PLA/Posidonia Oceanica Green Composites: A Simple Model Based on Starting Morpho-Chemical Properties. *Compos. Sci. Technol.* **2021**, *213*, 108930.
(43) Maio, A.; Gulino, E. F.; Gammino, M.; Citarrella, M. C.; Scaffaro, R. Photochemical Degradation of PLA-Based Green Composites Containing Waste Biomass from Posidonia Oceanica, Chamaerops Humilis and Ailanthus Altissima: A Comparative Study. *Polym. Degrad. Stab.* **2025**, *234*, 111204.
(44) Meier, M. A. R.; Subramaniam, B.; Moores, A.; Loh, W.; Biddinger, E. J.; Hwang, B. J.; Satoh, K.; Newton, G. N.; Handa, S.; Yan, N.; Hii, K. K. M.; Marr, A. C.; Hermans, I.; Leonard, K. C.; Carrier, D. J.; Chen, J.; Santato, C.; Brady, D.; Srubar, W. V.; Shastri, Y.; Nakamura, R.; Gathergood, N.; Han, H.; Serrano, J. F.; Licence, P. Expectations for Manuscripts in the Field of Polymer Science in *ACS Sustainable Chemistry & Engineering*. *ACS Sustainable Chem. Eng.* **2025**, *13* (8), 3022–3023.
(45) Hao, C.; Liu, T.; Zhang, S.; Brown, L.; Li, R.; Xin, J.; Zhong, T.; Jiang, L.; Zhang, J. A High-Lignin-Content, Removable, and Glycol-Assisted Repairable Coating Based on Dynamic Covalent Bonds. *ChemSusChem* **2019**, *12* (5), 1049–1058.
(46) Barros, A.; Nepomuceno, N.; Nicácio, P.; Souza, M.; Silva, I.; Luna, C.; Fook, M.; Araújo, E.; Wellen, R. Enhancement of Biobased Epoxy Through the Curing and Thermal Stability Control with Carboxylic Acids. *J. Polym. Environ.* **2024**, *32* (5), 2431–2447.
(47) Cherif, L. Y.; Naar, N.; Mekki, A.; Ouadah, A.; Hamada, R. A.; Trache, D. Unlocking the Potential of Polylactic Acid: Exploring Its Thermal and Mechanical Properties for Vitrimerization via Double Reactive Extrusion and Transesterification. *J. Appl. Polym. Sci.* **2025**, *142* (11), e56603.
(48) Román, F.; Colomer, P.; Calventus, Y.; Hutchinson, J. Study of the Molecular Dynamics of Multiarm Star Polymers with a Poly(Ethyleneimine) Core and Poly(Lactide) Multiarms. *Materials* **2017**, *10* (2), 127.
(49) Corneillie, S.; Smet, M. PLA Architectures: The Role of Branching. *Polym. Chem.* **2015**, *6* (6), 850–867.
(50) Hayashi, M.; Yano, R. Fair Investigation of Cross-Link Density Effects on the Bond-Exchange Properties for Trans-Esterification-Based Vitrimers with Identical Concentrations of Reactive Groups. *Macromolecules* **2020**, *53* (1), 182–189.
(51) Grizzi, I.; Garreau, H.; Li, S.; Vert, M. Hydrolytic Degradation of Devices Based on Poly(DL-Lactic Acid) Size-Dependence. *Biomaterials* **1995**, *16* (4), 305–311.
(52) Zi, Y.; Wang, G.; Chen, D.; Yang, W.; Ma, Y. Vinylogous Urethane Vitrimers Derived from Styrene Copolymers for Reprocessable Damping Materials. *Ind. Eng. Chem. Res.* **2025**, *64* (46), 22274–22286.
(53) Gentile, M.; Gaeta, L.; Brenna, S.; Pellecchia, C. Efficient Chemical Recycling of Poly(L-Lactic Acid) via Either Alcoholysis to Alkyl Lactate or Thermal Depolymerization to L-Lactide Promoted by Zn(II) Catalysts. *Polym. Test.* **2025**, *143*, 108727.
(54) Pickering, S. J. Recycling Technologies for Thermoset Composite Materials—Current Status. *Compos. Part A Appl. Sci. Manuf.* **2006**, *37* (8), 1206–1215.
(55) Liu, Y.-Y.; Liu, G.-L.; Li, Y.-D.; Weng, Y.; Zeng, J.-B. Biobased High-Performance Epoxy Vitrimer with UV Shielding for Recyclable Carbon Fiber Reinforced Composites. *ACS Sustainable Chem. Eng.* **2021**, *9* (12), 4638–4647.
(56) Xu, Y.; Dai, S.; Zhang, H.; Bi, L.; Jiang, J.; Chen, Y. Reprocessable, Self-Adhesive, and Recyclable Carbon Fiber-Reinforced Composites Using a Catalyst-Free Self-Healing Bio-Based Vitrimer Matrix. *ACS Sustainable Chem. Eng.* **2021**, *9* (48), 16281–16290.
(57) Yamaguchi, A.; Hashimoto, T.; Kakichi, Y.; Urushisaki, M.; Sakaguchi, T.; Kawabe, K.; Kondo, K.; Iyo, H. Recyclable Carbon Fiber-reinforced Plastics (CFRP) Containing Degradable Acetal Linkages: Synthesis, Properties, and Chemical Recycling. *J. Polym. Sci. Part A Polym. Chem.* **2015**, *53* (8), 1052–1059.
(58) Cunha, I. T.; McKeeman, M.; Ramezani, M.; Hayashi-Mehedy, K.; Lloyd-Smith, A.; Bravi, M.; Jessop, P. G. Amine-Free CO_2 -Switchable Hydrophilicity Solvents and Their Application in Extractions and Polymer Recycling. *Green Chem.* **2022**, *24* (9), 3704–3716.